Coupling between plasmonic films and nanostructures: from basics to applications

Thomas Maurer, Pierre-Michel Adam, Gaëtan Lévêque

Review article

Thomas Maurer*, Pierre-Michel Adam and Gaëtan Lévêque

Coupling between plasmonic films and nanostructures: from basics to applications

Abstract: Plasmonic film-nanoparticles coupled systems have had a renewed interest for the past 5 years both for the richness of the provided plasmonic modes and for their high technological potential. Many groups started to investigate the optical properties of film-nanoparticles coupled systems, as to whether the spacer layer thickness is tens of nanometers thick or goes down to a few nanometers or angstroms, even reaching contact. This article reviews the recent breakthroughs in the physical understanding of such coupled systems and the different systems where nanoparticles on top of the spacer layer are either isolated/random or form regular arrays. The potential for applications, especially as perfect absorbers or transmitters is also put into evidence.

Keywords: surface plasmon polaritons; localized surface plasmons; plasmonic coupling; metallic film; absorbers; gap modes.

DOI 10.1515/nanoph-2014-0015
Received July 25, 2014; accepted January 19, 2015

1 Introduction and basics

Plasmonics emerged mostly in the 1990s as an extremely rich new domain in optics, exciting due to its many applications ranging from simply down-scaling the conduction of light in subwavelength devices [1], to designing nanosources of light [2], new single-molecules biosensors [3], developing innovative treatment in cancer therapy [4], efficient and cheap solar cells [5], or designing an entirely new type of metamaterials, where "atoms" are artificially built as complex optical nanostructures allowing for the manipulating of light at will in ways not found in nature [6]. Specifically, surface plasmons are optical modes bound to the interface between a dielectric and a metal nano-object, which originate from the resonant coupling between a surface-charge oscillation and the electromagnetic field that it scatters. The wavelength at which the resonance takes place depends on the geometry, the nature and the environment of the system; the electromagnetic field is then concentrated and enhanced within a subwavelength distance to the interface. On the one hand, extended metal interfaces support so-called delocalized, or propagative, surface plasmon (PSP) modes, which are surface waves traveling along the interface of distances in the micrometer range, depending on the nature of the metal, the wavelength of the incoming light and the adjacent material [1]. On the other hand, metal nanoparticles support optical modes called localized surface plasmons (LSPs) [7]: for one or several specific wavelengths, an incoming electromagnetic wave will have its intensity enhanced in a volume of very small extension around the particle (usually a few ten nanometers for wavelengths in the visible spectral range), experimentally observed through an increase in the absorption and/or scattering cross-sections of light. The nature of those modes, their resonance wavelengths and widths, as well as the enhancement factor and the localization volume depend on the shape, metal, volume and environment of the nanoparticle. A specific feature of localized surface plasmons is the squeezing of the optical field in very small volumes (a few nanometers) which leads to the formations of "hot-spots", usually localized at sharp tips of metal particles [8] or inside gaps of a particle dimer [9] or in between a metal particle and a metal film.

At the merging of these two extreme cases, coupled film-nanoparticles plasmonic systems have experienced a

***Corresponding author: Thomas Maurer,** Laboratory of Nanotechnology and Optical Instrumentation, UMR 6281 STMR, Technological University of Troyes, 12 Rue Marie Curie, CS 42060, 10004 Troyes Cedex – France, e-mail: thomas.maurer@utt.fr
Pierre-Michel Adam: Laboratory of Nanotechnology and Optical Instrumentation, UMR 6281 STMR, Technological University of Troyes, 12 Rue Marie Curie, CS 42060, 10004 Troyes Cedex – France
Gaëtan Lévêque: Institut d'Electronique, de Microélectronique et de Nanotechnologie (IEMN, CNRS-8520), Cité Scientifique, Avenue Poincaré, 59652 Villeneuve d'Ascq, France

Edited by Volker Sorger

renewed interest for the past 5 years, both for the richness of the provided plasmonic modes and for their high technological potential. Many groups have started to investigate optical properties of film-nanoparticles coupled systems, whether the spacer layer thickness is tens of nanometers thick or goes down to a few nanometers or angstroms, even reaching contact. This article reviews the recent breakthroughs in the physical understanding of such coupled systems and the different systems where nanoparticles on top of the spacer layer are either isolated/random or form regular arrays. After a brief overview of the plasmonic properties of nanoparticles and their extended systems, the interaction between a metal film and regular arrays of metal nanoparticles are reviewed. Then, attention is focused onto single/random metal nanoparticles interacting with a plasmonic film and eventually, examples of potential applications, especially perfect absorbers and transmitters, are detailed.

1.1 Localized surface plasmons modes

The qualitative aspect of the plasmons modes of a single metal nanoparticle particle is extremely dependent on its shape and size. A nanosphere does not have the same kind of localized plasmons modes as a nanocube or a nanodisk, which will affect the way these particles couple to a metal film.

In the electrostatic approximation, which corresponds to a particle with a size much smaller than the wavelength in the embedding dielectric, retardation effects can be neglected. A metal nanosphere of permittivity $\varepsilon(\lambda)$ in an homogeneous dielectric of permittivity ε_B presents one dipolar resonance whose wavelength is given by $\varepsilon(\lambda)\approx -2\varepsilon_B$. When the size of the particle increases, retardation effects cannot be omitted, and the optical response of the metal particle must be studied by fully resolving Maxwell's equations, for example, by expanding the electromagnetic field on the basis of vectorial spherical harmonics [5]. The plasmon modes of a nanosphere are labeled by only one number l and have angular frequencies ω_l. The lowest order l=1 corresponds to the dipolar mode, the number l=2 to the quadrupolar mode, l=3 hexapolar and so on. As an illustration, Figure 1A shows the extinction spectra computed using the Mie theory [10] of a spherical gold particle in water, with increasing radius up to R=100 nm. When R is small enough, only the dipolar mode appears around λ=520 nm, which shifts to the red with increasing radius. However, the quadrupolar mode at shorter wavelengths appears as a shoulder on the main dipolar resonance for R>50 nm. Similar spectra are obtained with a silver nanosphere in air, as shown on Figure 1B for R=60 nm [5]. If both dipolar (labelled TM_1) and quadrupolar modes (labelled TM_2) appears in the extinction spectrum, it is important to notice that the scattering spectrum is dominated by the dipolar mode, whereas the quadrupolar dominates the absorption spectrum. Such a striking difference comes from the fact that the quadrupolar mode has a weak net dipole momentum compared to the dipolar mode, which can be easily verified by the distribution of

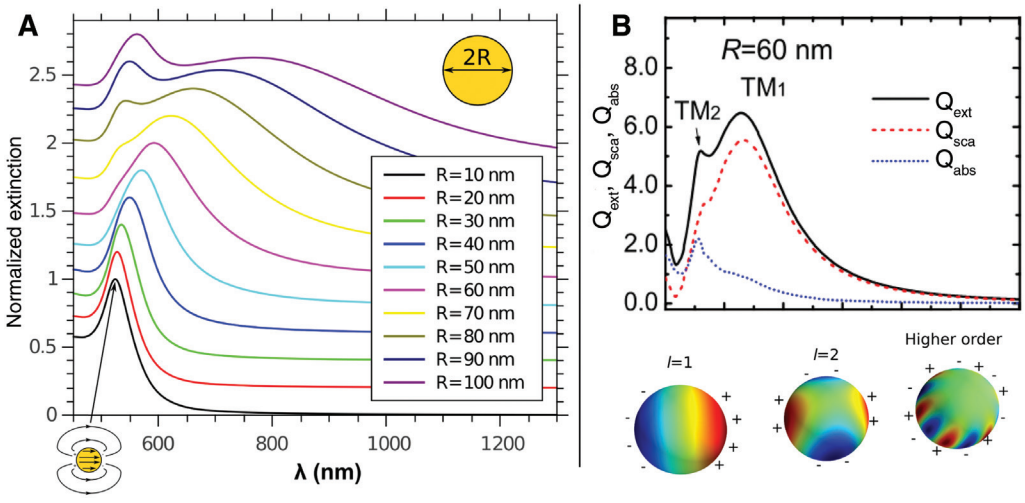

Figure 1: (A) Extinction spectra of gold nanospheres of increasing radius R in water, computed with the Mie theory; (B) extinction, scattering and absorption spectra of a 60-nm-radius silver nanosphere in air, together with the distribution of the surface charges for the dipolar, quadrupolar and an arbitrary higher order mode [5]. © IOP Publishing. Figure 1 (B top) reprinted from S. Hayashi and T. Okamoto, Journal of Physics D: Applied Physics, vol. 45. p. 433001, 2012. Reproduced by permission of IOP Publishing. All rights reserved.

the charges at the surface of the nanoparticle (Figure 1B, bottom right). This is an important characteristic as it will first determine if the mode can be efficiently excited from the far-field (it will then be also observable from the far-field by its scattered light), and it will modify the width of the plasmon resonance. In general, plasmon modes with a non-zero dipolar momentum, called "bright modes", will be broader than plasmon modes with weak dipolar momentum, called "dark" modes, the latter losing energy only by internal dissipation, whereas the former loses energy both by internal dissipation and scattering.

The plasmon modes of a metal nanocube are very different from the modes of a metal sphere. Following the seminal work by Fuchs in 1975 [11] who computed the bright modes of a ionic cube in the quasistatic approximation, Zhang et al. [12] investigated bright and dark modes of a silver nanocube in air, using the finite element method (see Figure 2A). The distribution of the surface charges on the cube interface shows clearly the distinction between bright (modes i to vi, non-zero dipolar momentum) and dark modes (modes vii and viii, zero dipolar momentum). Note that the mode analysis has also been made in the quasi-static approximation with the side of the cube equal to 3 nm for wavelengths in the UV range: there is no radiation loss and the resulting resonances are very thin as the internal losses in silver are very small. Bright modes correspond to both Fuchs and Zhang's work.

In general, dark modes cannot be easily seen by extinction spectroscopy as they are weakly excited by an incident plane wave. However, they can be detected by electron energy losses spectroscopy (EELS), as in the work by Schmidt et al. [13] where both bright and dark modes have been shown in silver nanodisks. The spectra obtained experimentally depend on the position at which the electron beam is focused, where the mode must have a non-zero field. Comparisons between the experimental spectra and numerical simulations (Figure 2B, top) have permitted the identification of the multipolar modes equivalent to the modes of a metal nanosphere (dipolar, quadrupolar, hexa, see the distribution of surface charges on Figure 2B, bottom). However, new modes specific to the cylindrical shape have been shown, labelled (0, 1) (dark) and (1, 1) (bright) on Figure 2B. The (0, 1) mode is a radial breathing dark mode, with which the electron coupling is the strongest.

Under certain conditions, the interaction between two localized surface plasmon modes can give rise to a so-called Fano resonance, characterized by an asymmetric profile in the extinction spectrum, where on the contrary a single dipolar mode will give a broad symmetric profile [14]. Usually, Fano resonance occurs when a narrow dark mode weakly couples to a wide bright mode. For example, when a silver nanocube of few ten nanometers side is placed near a dielectric interface, the uncoupled dipolar and quadrupolar modes (resp. modes i and vii on Figure 2A) interact through the field reflected by the interface. Without the interface, the different symmetry of the two modes prevents them from any coupling. They will form two modes, one mostly dipolar (D, surface charges max near the interface) and

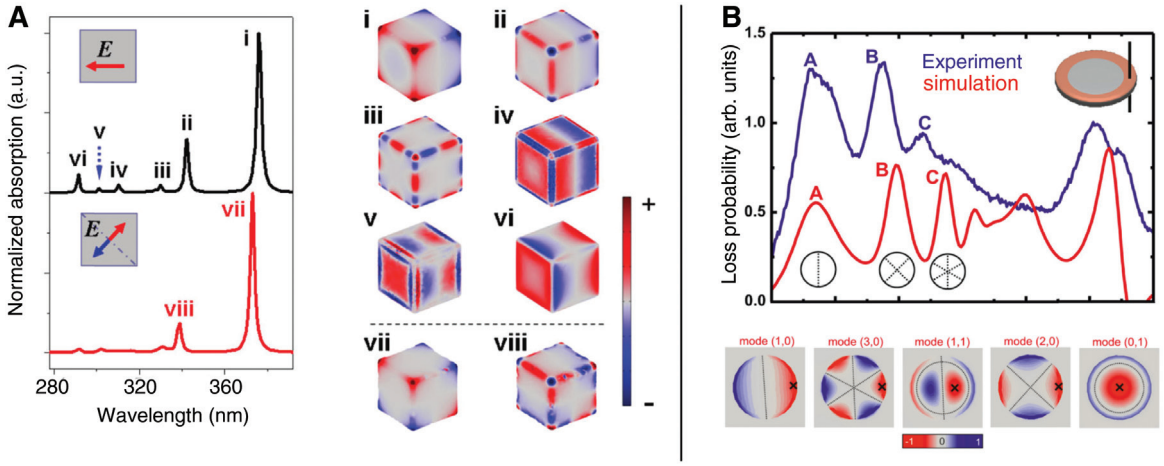

Figure 2: (A) Localized surface plasmon modes of a silver nanocube of 3 nm side length, in air [12]. Modes i to vi are bright modes with non-zero dipolar momentum; modes vii and viii are dark modes with no net dipolar momentum; (B) top: EELS spectrum of silver nanodisks for an electron beam focused near the edge of the particle; bottom: distribution of the surface charges associated with each LSP mode of the nanodisk identified as a maximum in the EELS spectra [13]. Reprinted with permission from Nano Lett., 2011, 11 (4), pp 1657–1663 and Nano Lett., 2012, 12 (11), pp 5780–5783. Copyright 2011 and 2012 American Chemical Society.

one mostly quadrupolar (Q, surface charges max away from the interface). A characteristic Fano profile appears inside the extinction spectrum when the peaks of the Q and D modes overlap, that is, when the distance between the Q and D modes is smaller than the width of the D mode, which occurs when the D^0 and Q^0 modes overlap and for moderate substrate dielectric constant and particle-substrate distance. However, Fano profiles can also form between two bright modes [15], as demonstrated by Lovera et al. in the investigation of a structure composed of a nanoantenna coupled to a system of two parallel nanorods (Figure 3A).

A very important application of Fano profile is their potential use in LSP-based biosensors. Compared to PSP-based sensors, they could allow for many portable devices, they need a lower number of molecules to achieve a measurable shift, and could have a lower cost and be much simpler to use. However, the width of the plasmon resonance and the smaller bulk refractive indexes sensitivity leads to lower resolution than delocalized surface plasmon sensors. In this context, the Fano resonances are very attractive because of their narrow width. For example, Verellen et al., have demonstrated that large figures of merit could be achieved in a system consisting in gold nanocrosses coupled to gold nanobars [16]: the principle is to induce a coupling between the dark mode supported by the nanocross and the bright mode supported by the nanobar, which leads to a large refractive index sensitivity of about 1000 nm/RIU together with a FoM of about 5, operating at a wavelength of 1 μm.

1.2 Propagative surface plasmon modes

Contrary to localized surface plasmon, delocalized or propagative surface plasmons were discovered at the beginning of the 20th century by Robert Wood, as an anomaly in the spectrum of the light reflected from a metallic diffraction grating. This late discovery may be attributed to the fact that propagative surface plasmons modes are evanescently bound to the metal dielectric interface (Figure 4A) and as such cannot be excited from or observed in the far-field [1]. As they are propagative modes, they obey a dispersion relation relating the angular frequency ω to q(ω), the component of the wavevector of the surface plasmon mode parallel to the metal-dielectric interface. The evanescent decay of the wave amplitude perpendicular to the interface in the dielectric comes from the fact that $q(\omega)>n_B k_0$, which makes $k_z=\sqrt{(\varepsilon_B k_0^2-q(\omega)^2)}$ imaginary. As a consequence, the surface mode, on a completely flat interface, can only be excited with an evanescent wave. Kretschmann paved the way in the 1970s to a deeper investigation of the PSPs

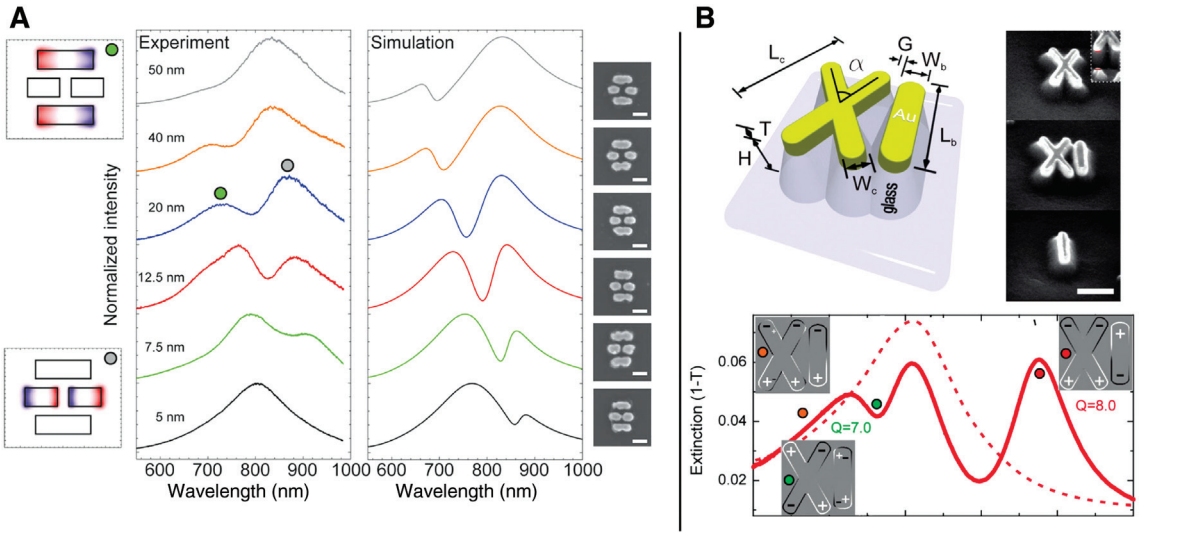

Figure 3: Different types of Fano profiles resulting from the interference between localized plasmon modes supported by two plasmonic systems. (A) The Fano profile appears when two bright modes interfer; (B) interference of a sharp dark mode supported by the X-shaped nanoparticle and the dipolar longitudinal bright mode supported by the nanobar. Indicated are the quality factors of the two resonances, much larger for the dark mode. The dashed line represents the superradiant envelop of the mode resulting from the antibonding combination of the dipolar modes associated to the cross and the nanobar. Reprinted with permission from ACS Nano, 2013, 7 (5), pp 4527–36. Copyright 2013 American Chemical Society.

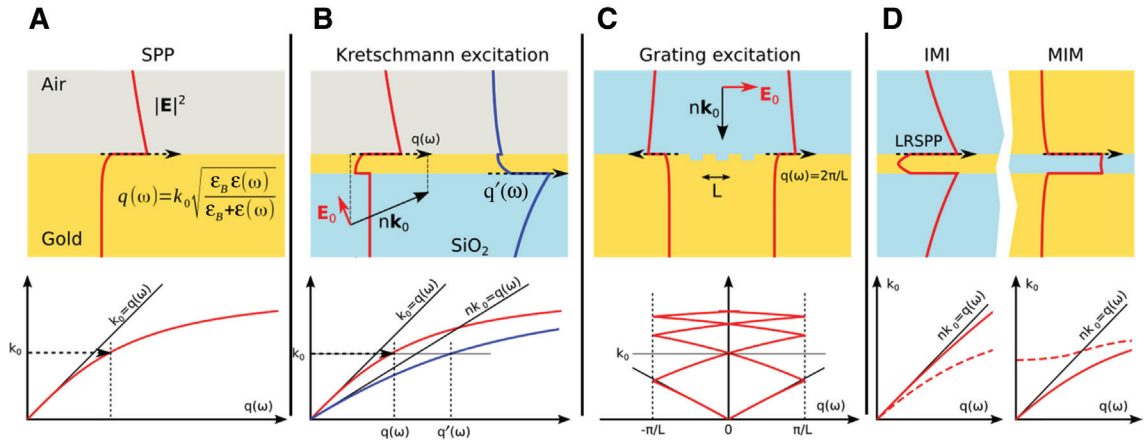

Figure 4: (A) Top: intensity profile of a typical PSP mode, propagating at angular frequency ω and with parallel wavevector q(ω) along an interface between a metal and air; Bottom: dispersion curve of the plasmon mode, which lies outside the light cone of air. (B) Top: intensity profiles of the two PSP modes in the Kretschmann configuration. The metal-air surface plasmon can be excited sending a planewave from the higher index substrate in total internal reflection; Bottom: dispersion curves of the two plasmon modes. (C) Top: grating coupler for PSP excitation. The period must be on the order of $2\pi/q(\omega)=\lambda_{PSP}$ for a planewave in normal incidence. Bottom: in the approximation of a weak coupling between the grating and the PSP, the dispersion relation of (A) is simply folded inside the first Brillouin zone. (D) Intensity profiles and dispersion curves (solid lines) of the antisymmetric, long range PSP in the insulator-metal-insulator (IMI) configuration, together with antisymmetric PSP mode in the metal-insulator-metal (MIM) configuration. Dashed lines correspond to the short range PSP (IMI) and the symmetric PSP (MIM).

properties by proposing a very convenient way to excite them through evanescent-wave coupling (Figure 4B). In this configuration, a thin metal film, deposited on a silica substrate, is illuminated in total internal reflection from the substrate: the parallel component of the incident light wavector is then increased and can excite the PSP on the metal-air interface, while the metal-substrate PSP remains not radiatively coupled to either of the adjacent dielectric and not excitable from the far-field. For a given wavelength, the air-metal PSP excitation is then angle-specific, this angle depends on the film thickness and the media above and under the film, more specifically in the area few ten nanometers above the film where the surface wave extends. This is the basics of LSP sensing, widely used for the last 20 years since the pioneering work of Nylander et al. [17].

An alternative and very common way of PSP excitation is the use of a localized defect, which allows to increase the parallel component of the wavevector of an incident planewave by diffraction [18], the ideal system being a diffraction grating for which the period L allows the wavevector matching with the plasmon momentum. In the weak coupling limit, the dispersion relation of the PSP is simply folded inside the first Brillouin zone, and the matching one occurs when, at the selected angular frequency, the parallel component $k^x_{//}$ of the incident planewave obeys $q(\omega)=k^x_{//}+m2\pi/L$ for a 1D grating with period along the x direction, for a given integer m (Figure 4C). This configuration has been efficiently used in order to build unidirectional coupler and focusing elements [19], or excitation of PSPs propagating along metal tip for tip-enhanced-Raman-spectroscopy (TERS) applications [20]. Lamy et al., demonstrated experimentally in 2011 that PSPs can be directly excited on the top surface of a metalized single-mode vertical cavity surface emitting-laser (VCSEL), permitting the propagation and manipulation of the PSP on a compact integrated device [21]. Finally, periodic structuration of a metal film by holes has led to the observation of the so-called “extraordinary transmission” effect, in which the amount of light transmitted through the structured metal is larger than the amount of light transmitted by the equivalent area of the holes. This effect is attributed mostly to the surface plasmons excitation together with slower decaying “creeping waves” due to the short distance between the holes compared to the PSP propagation length [22].

Finally, interesting properties are obtained when identical delocalized surface plasmons are coupled together, leading to symmetric and antisymmetric combinations of the uncoupled PSPs. Two basic configurations are possible: in the insulator-metal-insulator (IMI) structure, a thin film of metal is placed in between two identical dielectric over- and under-coatings, whereas in the metal-insulator-metal (MIM) configuration (Figure 4D), a thin dielectric gap lies in between two identical metals. In the IMI

configurations, the metal film is typically made of gold, with a thickness about 20 nm (for visible wavelengths), and the two symmetric and anti-symmetric delocalized plasmon modes (we refer to the symmetry of the full electric field vector) are called, respectively, short-range and long-range surface plasmon modes. In the anti-symmetric mode, the electric field is mostly expelled from the metal, hence reducing the internal losses and leading to longer propagation length [23]. Because of their larger field enhancement, their lower losses and penetration depth, those long-range surface plasmons have been proven to be an efficient way to improve the efficiency of PSP-based biosensors, allowing, for example, to sense large biological systems like cells or viruses [24]. Let us mention that an interesting connection can be done with the localized surface plasmons modes of a flattened parallelepiped particle, as it has been shown that the short-edge localized plasmon connects with the long-range surface plasmon when the particle length increases (not its thickness) to become a film, whereas the long edge localized plasmon connects to the short range surface plasmons [25]. The MIM configuration is fundamentally different to the IMI configuration as it can support waveguide modes for a large gap, however, only the antisymmetric plasmon modes persist for small gaps. Similarly to the IMI configurations, these modes allow to transport light on "large" distances in order to design plasmonic slot waveguides. Let us notice that when the gap decreases, the PSP wave vector increases, which means its effective wavelength, parallel to the interfaces, is reduced. This configuration is important in the study of metal particle-film system as such a MIM structures is naturally formed, for example, in between a flat cylindrical or rectangular particle and an extended metal film.

2 Plasmonic nanoparticle arrays coupled to films

2.1 Coupling with random arrays of particles (high coverage)

The first experiments ever reported on coupling between nanoparticles and metallic films were done on thermally evaporated islands by Holland and Hall [26]. Reflectivity spectra of silver and gold island films deposited on a continuous silver film via various thickness spacers of lithium fluoride LiF were measured in an attenuated total reflectance (ATR) configuration (Figure 5). Light wavelength is fixed and the incidence angle is monitored. In the absence of a spacer layer and metal islands the minimum of reflectance characterizes the excitation of a propagating plasmon or (PSP) on the silver film. The presence of the spacer layer and then of the islands/nanoparticles induce an angular shift on the PSPs resonance condition. The authors found that by measuring the ATR spectra for different incident wavelengths that the stronger angular shift was obtained when the wavelength was matching the LSP of the metal islands.

Similar results were later reported by Kume et al. [27] this time on a Ag-SiO2 composite deposited on top of an aluminum film with a SiO2 spacer layer (Figure 6). In addition to reflectivity measurements further information was obtained on the coupled system as scattered light is also detected above the islands films. This shows nicely the coupling between the PSP and the nanoparticles, where first PSP are excited through angular phase matching, secondly nanoparticles are excited through the evanescent field of the PSP and thirdly the induced dipole in the nanoparticles scatter light in air.

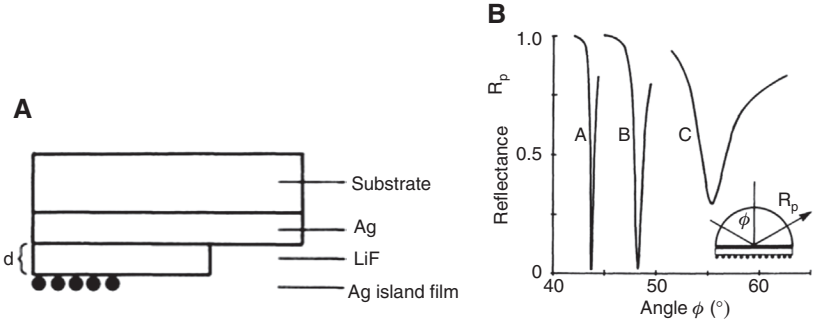

Figure 5: (A) Sample geometry used in the experiment of Holland and Hall [26]. The continuous silver film has a thickness of 50 nm. The thickness of the LiF spacer layer d was varied between 5 and 60 nm. The silver-island film had a mass thickness of 3 nm. (B) Measured reflectivity R_p, as a function of the angle in the prism. In this case, the excitation wavelength was 514.5 nm and the spacer-layer thickness d=20 nm. A: Ag-air; B: Ag-LiF-air; C: Ag-LiF-Ag islands-air. Insert shows ATR geometry. Reprinted figure with permission from W. R. Holland and D. G. Hall, Phys. Rev. B, 27, 7765–7768, 1983. Copyright (1983) by the American Physical Society.

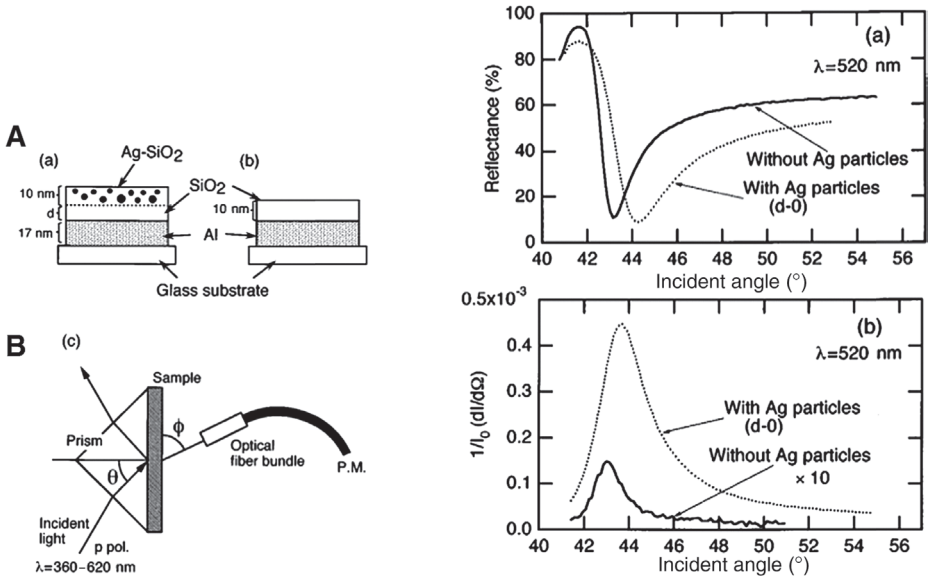

Figure 6: (A) and (B) Geometry of the samples in the experiment of Kume et al. [27]. (c) Experimental arrangement for measurements of light emission under PSP excitation. (C) ATR spectra and (D) dependences of emitted light for the sample with (d-0) and without Ag particles. The emitted light was measured fixing the observation angle of 90°. The wavelength of the incident light was set to 520 nm. Reprinted figure with permission from T. Kume, S. Hayashi, and K. Yamamoto, Phys. Rev. B, 55, 4774–4782, 1997. Copyright (1997) by the American Physical Society.

In later experiments Holland and Hall measured near-normal reflectance with light incident on the metal islands side on the same coupled system as represented in Figure 5 (left). This time there is no direct excitation of the PSP as there is no crossing between the curves of light dispersion in air and that of the PSP. Reflection spectra (Figure 7, left) show a deep minimum, which, in the asymptotic case where spacer layer is infinite, corresponds to the LSP of the silver islands. As the spacer layer is decreased (Figure 7, middle) the LSP resonance of the silver islands is first blue shifted (d>50 nm) and then red-shifted (d<50) nm.

Replacing silver islands with gold ones (Figure 7, right), these authors observed two minima at 350 nm and 540 nm. They assigned the 540-nm minimum to a gold particle LSP resonance and the 350 nm minimum to the excitation of a propagating surface-plasmon mode or PSP. The phycical mechanism of PSP excitation can be thus considered. Particles scatter light and if only far-field radiation is taken into

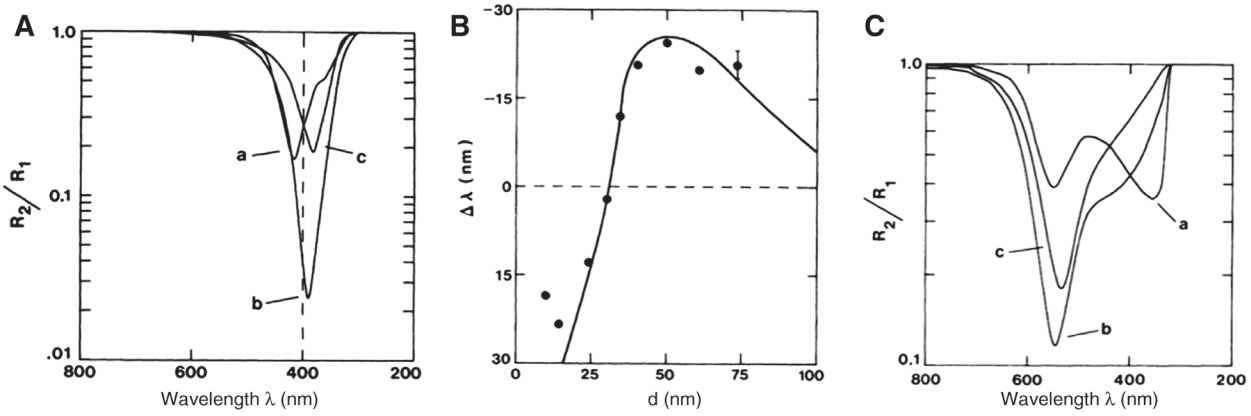

Figure 7: (A) Measured specular reflectance, in the experiment of Holland and Hall [28], of silver-island samples (normalized by Ag-LiF reflectance) as a function of wavelength for three different values of spacer-layer thickness d. Curve a, d=8 nm; curve b, d=27 nm; curve c, d=46 nm. (B) Variation of observed silver-island resonance wavelength shift with spacer-layer thickness. (C) Measured specular reflectance only with gold islands replacing the silver islands as a function of wavelength for three values of spacer-layer thickness. Reprinted figure with permission from W. R. Holland and D. G. Hall, Phys. Rev. Lett., 52, 1041–1044, 1984. Copyright (1984) by the American Physical Society.

account there is no phase matching possible with the PSP dispersion curve. Note here that due to the low thickness of the metal film one has to consider two dispersion curves due to coupled PSP on both interfaces, symmetric and antisymmetric PSP. However, when one considers the near-field of the scatterer, evanescent waves with high k vector are dominant in this subwavelength range. Thus phase matching is possible as long as the spacer layer thickness is lower than the penetration depth of the evanescent waves. This process of PSP excitation is nonetheless less efficient than grating coupling due to the broad spectrum of k vectors present in the near-field of the scatterer. However, in the case of a high density coverage of nanoparticles present on the surface as evidenced in thermal annealed samples, such a low efficient process for a single particle can be compensated by a high number of scatterers. It can also be noticed that the k spectrum of evanescent waves can be monitored if particles sizes and shapes are changed thus allowing a possible improved PSP coupling for a fixed spacer thickness.

We will now examine the coupling between particles and a metallic film in the case where now there is a spacer layer in between. Most interestingly the spacer layer itself can induce thickness-dependent effects on the LSP resonances of particles. Stuart and Hall reported experiments where metal islands were deposited on silicon-on-insulator (SOI) wafers. A thin LiF layer (30 nm) lies between the Ag islands and the SOI. Transmission spectrum of Ag islands on a LiF-coated glass substrate is measured as a reference and show the LSP of islands as a dip around 430 nm (Figure 8, left). When Ag islands are formed on SOI wafers photocurrent generation is measured as a function of the wavelength. The photocurrent spectrum is noticeably different from the reference and shows the strong particle-silicon waveguide coupling. The difference in the spectroscopy of two systems can be further seen when scattered light is recorded above the islands (Figure 8, middle). Coupling between the particles and the modes supported by the silicon waveguide modulates the LSP of the Ag islands by creating a series of dips and maxima in the LSP peak but also adding new peaks outside the LSP spectral window. The coupling can be seen as follows: the particles excite the waveguide modes through near-field interaction and the waveguides modes further excite the neighboring particles. As a final experiment Stuart and Hall investigated the role of a LiF spacer layer thickness placed between Ag islands and an Ag mirror (Figure 8, right). When LiF thickness is below 150 nm the system only supports the PSP mode on the Ag mirror with a strong redshift and broadening of the LSP resonance, while when the thickness is above 150 nm a new mode appear at lower wavelengths (TE01 mode of LiF layer) while the broad band is damped. In all cases interactions between particles and PSP or dielectric waveguides modes enhance the absorption of the system due to guided mode mediated particle interaction.

2.2 Coupling with ordered arrays/gratings of particles: no spacer

Here we will consider the coupling of ordered ensembles of particles to metal films. The first experimental

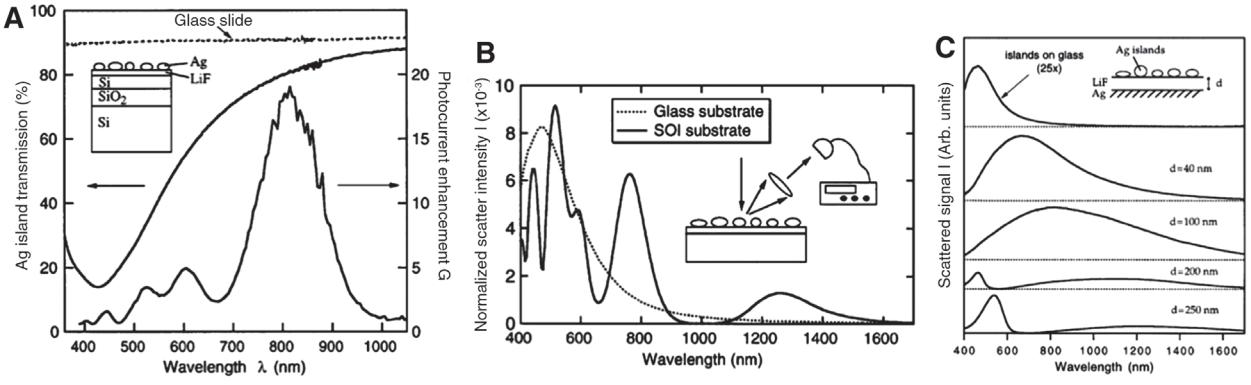

Figure 8: (A) Experiment of Stuart and Hall [29]. Transmission spectrum of a Ag-island film on a LiF-coated glass substrate, along with the measured photocurrent enhancement *G* produced by an identical Ag-island film formed on an SOI photodetector. The island-SOI structure is shown in the inset; the Si and SiO2 layer thicknesses are 160 and 200 nm, respectively. (B) Measured intensity of scattered light (normalized to the incident intensity) for a Ag-island film formed on LiF- coated glass (dotted line) and SOI (solid line). LiF thickness is 30 nm. (C) Measured intensity of scattered light (normalized to the incident intensity) for the Ag-islands/LiF/Ag-mirror geometry. The Ag-islands/LiF/glass signal is shown as the top curve, expanded by 25. Reprinted figure with permission from H. Stuart and D. Hall, Phys. Rev. Lett., 80, 5663–5666, 1998. Copyright (1998) by the American Physical Society.

demonstration of such an effect was demonstrated by Félidj et al. [30]. In this case there is no spacer layer and the authors used electron beam lithography (EBL) to fabricate well-controlled gratings of gold particles directly on a gold film, where sizes and shapes are very homogenous on a given array (Figure 9, left, inset). Particles here have a cylindrical shape and are thus called oblate spheroidal particles in reference to model structures for which an analytical description of the polarizability is known in the quasi-static approximation.

Extinction spectra are obtained in normal incidence (Figure 9, left). In the absence of a gold film particles they exhibit a single LSP in-plane resonance around 650 nm, due to their revolution axial symmetry. In the presence of the gold film two resonances appear at 525 nm and 650 nm. The coincidence of the long wavelength peak at 650 nm with the single peak obtained at the same wavelength in the case of no gold film is purely fortuitous.

The low wavelength peak at 525 nm was interpreted as an "isolated" LSP resonance of the particles and the long wavelength peak was attributed to a "collective" LSP resonance. Such a description of the two peaks seen in Figure 9 (left) is similar to the well-known and commonly observed two LSP peaks in the extinction spectra of aggregated colloids. However, in the sample of Figure 9 (inset) the distance between neighboring particles should not allow a direct coupling of LSP. Indeed, the lateral extension of the confined evanescent fields cannot induce this interaction. Collective LSP resonance is explained by the mediation of PSP excitation and interaction. In this physical picture PSP are excited through near-field coupling of nanoparticles to the film and as the attenuation length of the PSP is much higher than interparticle distance the PSP mediates the interaction between particles.

Further results (Figure 9, right) show that when only spacing or interparticle distance is changed for the same nanoparticles shapes and sizes a third resonance appears that red-shifts when this spacing is increased. This third peak appearing in the extinction spectrum when spacing between particles is varied (Figure 9, right) was interpreted in terms of stationary PSP. Such PSP excitation occurs when the wave vector is equal to half the grating vector, thus resulting in Bragg scattering inducing forward and backward traveling waves that interfere to form standing

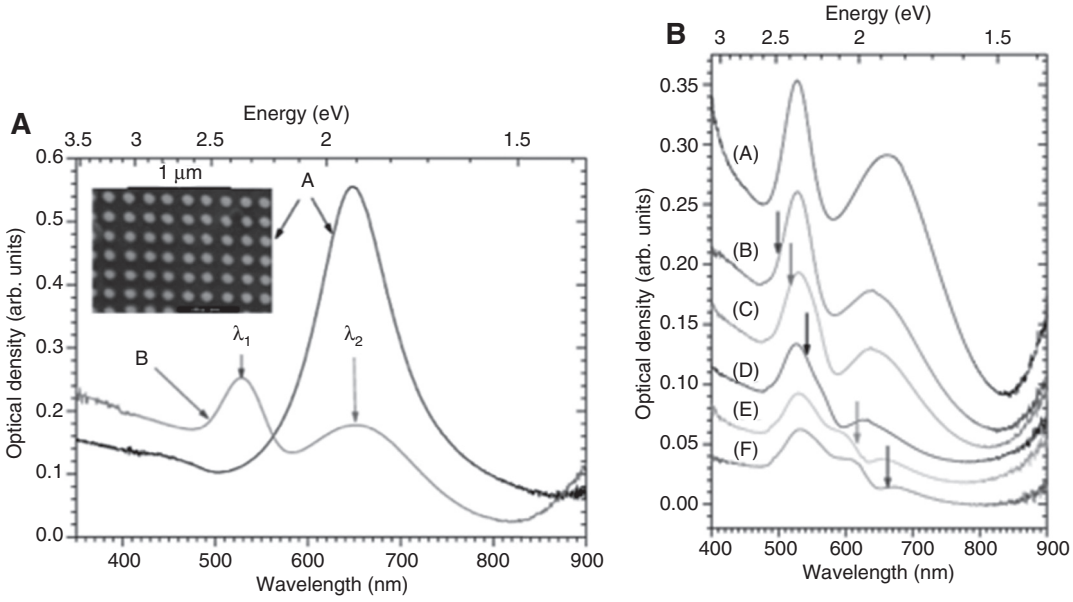

Figure 9: (A) Extinction spectrum of arrays of gold oblate spheroidal particles in the experiment of Félidj et al. [30], deposited on ITO, major axis 110 nm parallel to the ITO substrate, minor axis 60 nm perpendicular to the ITO, interparticle spacing 200 nm (spectrum *A*), and a 20-nm gold film, major axis 120 nm parallel to the gold film, minor axis 44 nm perpendicular the gold film, interparticle spacing 200 nm (spectrum *B*). The inset displays a scanning electronic microscopy image of the array of gold particles on ITO. (B) Extinction spectra of arrays of gold oblate spheroidal particles identical to those of spectrum *B*, deposited on a 20-nm gold film for different spacing between particles: spectrum *A*: 180 nm, spectrum *B*: 200 nm, spectrum *C*: 230 nm, spectrum *D*: 250 nm, spectrum *E*: 300 nm, spectrum *F*: 320 nm. Spectrum *F* is vertically lowered by 0.03 density unit for clarity. Arrows display the wavelengths at which the Bragg scattering condition is fulfilled. Reprinted figure with permission from N. Félidj, J. Aubard, G. Lévi, J. R. Krenn, G. Schider, A. Leitner, and F. R. Aussenegg, Phys. Rev. B, 66, 245407, 2002. Copyright (2002) by the American Physical Society.

waves. Stationary PSP are highly sensitive not only to spacing but to the height of the particles.

Additional experiments on similar samples (Figure 10A and B) were done by Hohenau and Krenn [31]. By varying the grating spacing between particles (Figure 10C) they clearly showed the distinction between two types of surface plasmon modes present in their extinction spectra. The spacing-insensitive mode at 525 nm was attributed to a vertical dipolar LSP resonance while the other peaks proved to be grating coupled PSP (Figure 10D). Due to the low thickness of the gold film (25 nm) one has to consider here coupled interfaces with both symmetric and antisymmetric PSP. Note that in contrast to our previous definition of these coupled PSP modes based on the symmetry of the electric field, here in the work of Hohenau and Krenn PSP modes are defined by the symmetry of the tangential magnetic field with respect to the gold-film plane. Only antisymmetric PSP (called symmetric PSP if defined with respect to the electric field) could be excited as symmetric PSPs called antisymmetric PSP if defined with respect to the electric field) energy is above interband transition level.

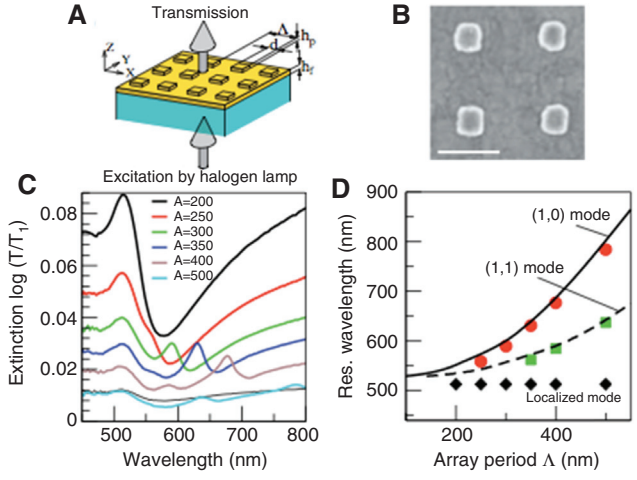

Figure 10: (A) Sketch of the sample and geometry of the experiment of Hohenau and Krenn [31]. The samples are illuminated from the glass-substrate side, the transmitted light is collected by a 2.5×, 0.075 numerical aperture objective and analyzed by a spectrometer; (B) exemplary SEM image; (C) extinction spectra of particle arrays with varying array periods. The reference for calculating the extinction is taken on the gold film outside the arrays. The thin line depicts the extinction spectrum of a sample with random particle distribution; (D) resonance wavelengths of the extinction peaks vs. array period: experimental values from (C) (symbols) and calculated values (lines) of different grating orders. Reprinted from Plasmonic modes of gold nano-particle arrays on thin gold films, Phys. status solidi – Rapid Res. Lett., 2010, 4, 256–258. Copyright Wiley-VCH Verlag GmbH & Co. KGaA. Reproduced with permission.

2.3 Coupling with gratings of particles: with a spacer

Coupling of ordered arrays of nanoparticles to waveguides modes of a spacer layer were reported by Linden et al. [32] where shapes and sizes of particles are controlled by EBL nanofabrication (Figure 11, left). Waveguide modes of the ITO layer are excited through grating coupling induced by the nanoparticles arrays. The waveguide modes excitation modulates the LSP broad band of the nanoparticles by a creating a series of peaks and dips (Figure 11, right). Grating coupling of the waveguide modes is definitely evidenced when the interparticle distance is changed in one direction of the 2D grating. When spacing is varied the series of peaks and dips is shifted as can be seen in Figure 11 (right).

Coupling between ordered arrays of nanoparticles and a metallic film were investigated by Cesario et al. [33], where the ITO acts as a spacer layer (see Figure 12).

The higher wavelength peak is interpreted by the grating coupling excitation of the lower PSP branch (1,0). The shift with the periodicity is similar to that described above in the no spacer case by Hohenau and Krenn [31]. The lower wavelength peak is mainly attributed to the LSP resonance of the array of nanoparticles.

Similar resonances are thus found in the presence and in the absence of spacer for coupled nanoparticles-films systems where both LSP and grating induced PSP are observed for sufficiently thin spacer thicknesses where no waveguide modes can be excited in the spacer itself. However, even for low thickness spacer layers some intriguing features are specific to each system. As mentioned by Félidj et al. [30] Bragg induced that stationary PSP can exist on nanoparticles on films where both periodicity and particle height will play a role. Furthermore in spacer separated systems gap modes can occur where the field can be confined in the gap between the particles and the film. New modes can thus appear, specific to this system as shown by Farhang et al. [34]. The distribution of charges on the particles and the film can display the nature of these new modes (Figure 13).

3 Single plasmonic nanoparticle coupled to films

In this section, we focus on the gap-dependent properties of a single metal particle coupled to a metal film, which is very similar to the properties of an assembly of randomly deposited particles in the low-coveraged limit.

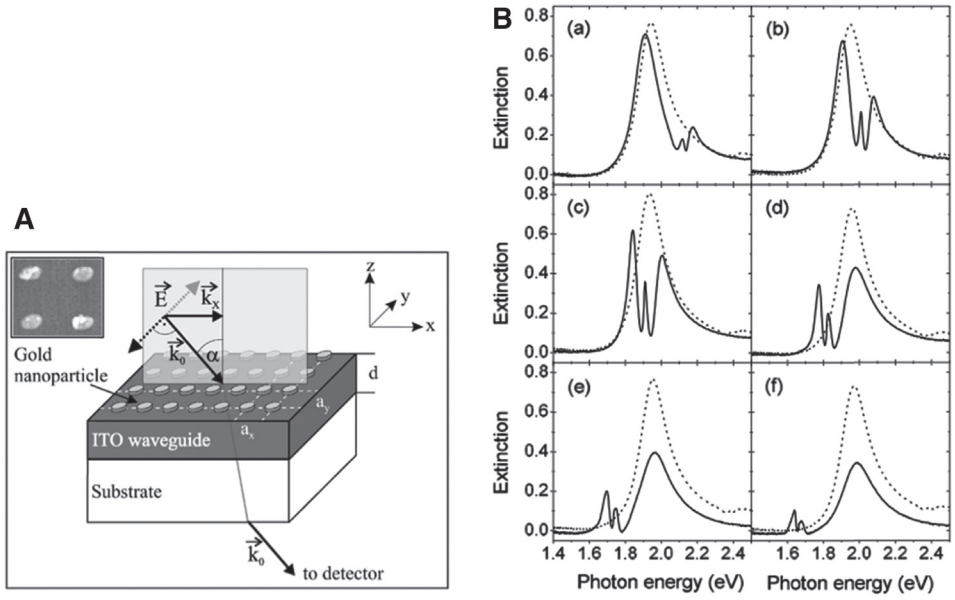

Figure 11: (A) Sketch of sample geometry. Inset: SEM picture of a gold nanoparticle array on a 140-nm-thick ITO waveguide. (B) Extinction of gold nanoparticles on a 140-nm-thick ITO waveguide. Solid lines: arrays with a fixed periodicity of 300 nm along the y axis and increasing periodicity from 350 nm to 475 nm in steps of 25 nm (A)–(F) along the x axis. Dashed lines: reference arrays with a periodicity of 300 nm for both axes. Reprinted figure with permission from S. Linden, J. Kuhl, and H. Giessen, Phys. Rev. Lett, 86, 4688–4691, 2001. Copyright (2001) by the American Physical Society.

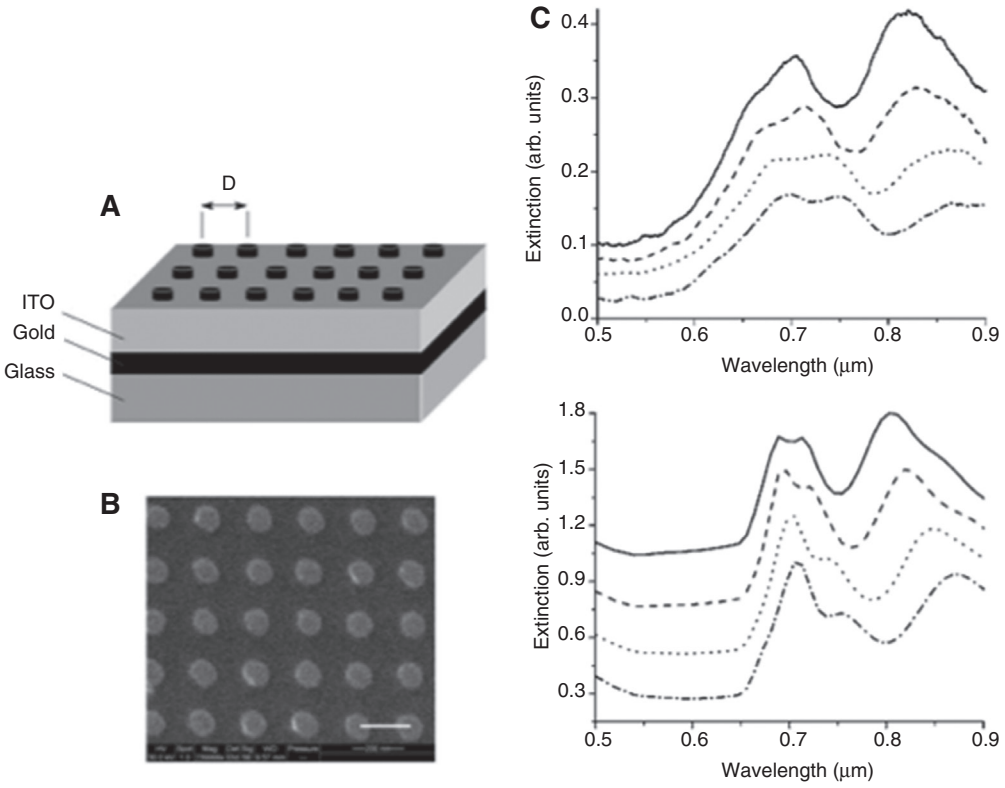

Figure 12: (A) Schematic description of the sample and (B) scanning electron micrograph of the top side (scale bar of 200 nm). (right) Extinction spectrum evolution with pitch *D* for the system (gold particle grating/ITO/gold layer). (C) Experimental, (D) theoretical. In both cases the curves have been translated vertically for further clarity. Reprinted figure with permission from J. Cesario, R. Quidant, G. Badenes and S. Enoch, Opt. Lett., vol. 30, no. 24, pp. 3404–3406 (2005). Copyright 2005 by the Optical Society (OSA).

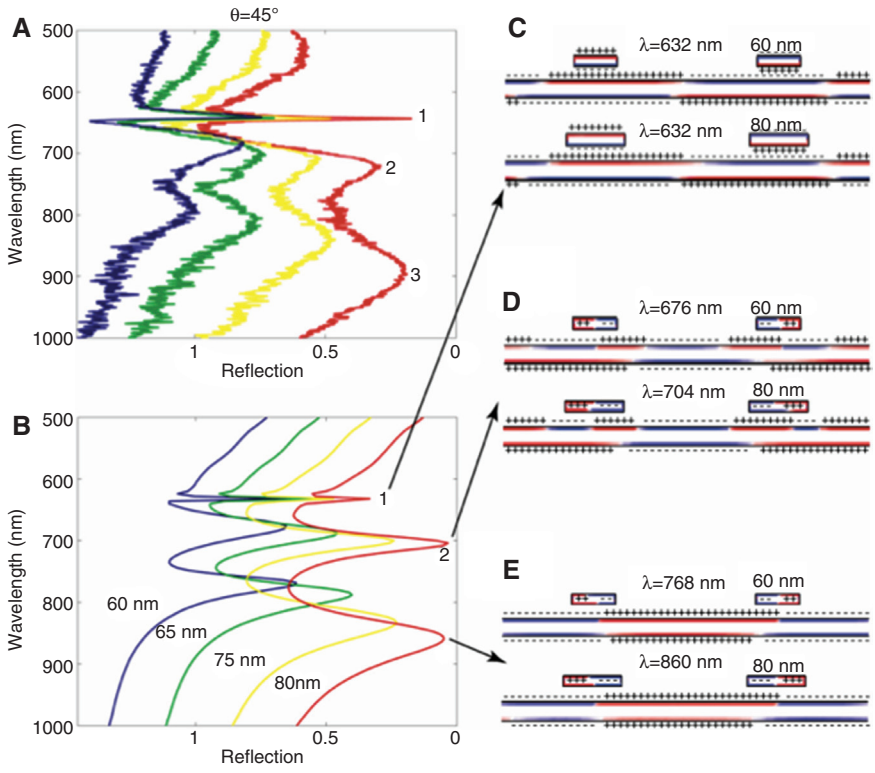

Figure 13: (A) Measured and (B) simulated reflection spectra at θ 1/4 45 deg incidence for gratings of widths w 1/4 80, 75, 65, and 60 nm. Each curve is displaced by an amount of 0.2 from the previous one for viewing purposes. (C) Surface charges for band 1 showing an odd surface plasmon-polariton (PSP) resonance. (D) Surface charges for band 2 showing a parallel hybridization combination of the even/compound PSP and the localized dipole+mirror image resonance. (E) Surface charges for band 3 showing the antiparallel hybridization combination. Reprinted figure with permission from A. Farhang, T. Siegfried, Y. Ekinci, H. Sigg, and O. J. F. Martin, "Large-scale sub-100 nm compound plasmonic grating arrays to control the interaction between localized and propagating plasmons," J. Nanophotonics, vol. 8, p. 083897, 2014. Copyright 2014 by SPIE.

3.1 Short distance coupling

Lassiter et al., have investigated experimentally and numerically the regime where the coupling distance is well below the wavelength, down to 5 nm [35]. The structure is composed of chemically grown silver cube of 80-nm side separated from a 50-nm-thick gold or silver film by alternating polyelectrolyte layers of poly(allylamine hydrochloride) (PAH) and polystyrene sulfonate. The constituted dielectric layer has a refractive index of 1.4 and its thickness can be varied on the nanometer scale through the layer-by-layer deposition process (Figure 14A, left). Dark-field spectroscopy combined with finite element method allowed showing that for both polarization (TM and TE) the structure exhibits one plasmon resonance in the visible which is red-shifted when the polymer thickness decreases or the cube side increases. When the gap is very small, the resonance corresponds to the excitation of a MIM-type PSP (MIMPSP in the following) mode localized in between the cube bottom and the metal film, see Part 1 (Figure 14A, bottom right, mode number 4). The strong impedance mismatch at the edge of the cube reflects the MIMPSP back inside the gap and creates a stationary wave, making the resonance occur when the cube length is about half the MIMPSP wavelength inside the dielectric. Numerical simulations have shown that higher order MIMPSP-resonances take places in the UV range (Figure 14A, mode number 1–3). Beside these MIMPSP modes, the authors showed, by looking at the evolution of the single cube modes wavelength with decreasing the gap thickness, that a localized dipolar plasmon mode always exists and is perpendicular to the interface. However, this mode becomes rapidly much damped compared to the MIMPSP mode when the gap decreases.

In this previous work, the localized plasmon modes of the system were observed by dark-field spectroscopy, so only the modes that can be radiatively coupled to light (or "bright") are excitable, without giving any insight about possible dark modes supported by the structure.

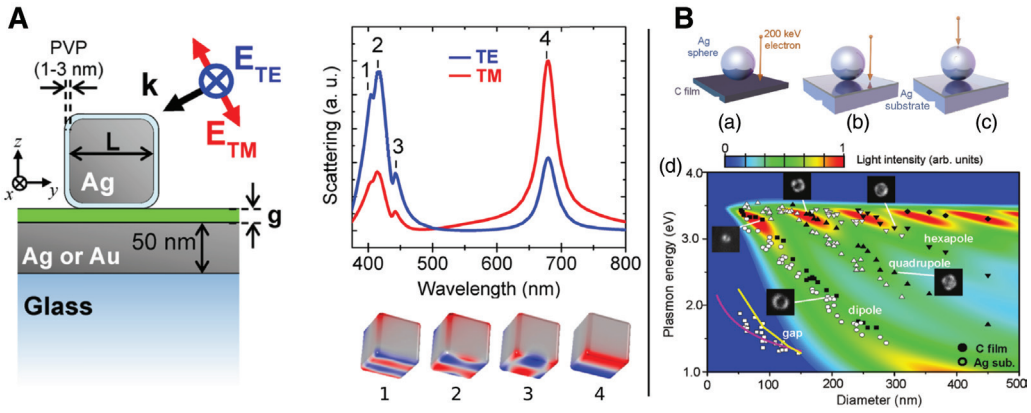

Figure 14: (A) Left: system investigated in [35], constituted by a 80-nm silver nanocube separated from a silver/gold film by a thin dielectric layer of alternating layers of PAH and polystyrene sulfonate. The silver cube is covered by a 3 nm-thick layer of aluminum oxide and excited by a plane wave in oblique incidence; Right: computed scattering spectra for the two incident polarizations (top) and distribution of the surface charges for each of the four modes indicated (bottom); (B) Top: investigated system in [36], constituted by a silver nanosphere placed on top of a carbon or silver substrate, with the position of the incident electron beam; Bottom: the colormap shows the calculated cathodoluminescence intensity from self-standing particles under grazing incidence, together with the experimental position of the Mie- and gap-plasmon modes obtained by EELS on carbon and silver substrate. The yellow and magenta curves are the size-dependent gap-plasmon position obtained from analytical and numerical simulations, respectively. Reprinted with permission from Nano Lett., 2013, 13 (12), pp 5866–5872. Copyright 2013 American Chemical Society.

Again, localized excitation with an electron beam, like in EELS spectroscopy, allows to more completely characterize the modal behavior of the particle-film system, as demonstrated in 2011 by Yamamoto et al. [36]. In this work, the authors use spectral cathodoluminescence, on a system composed of a silver nanosphere of varying diameter deposited either on a TEM carbon film or on a 200-nm silver layer. In this technique, the light emitted by the structure under localized electron beam excitation can be analyzed both as a function of the wavelength and the emission angle. Here, the 200 keV electron beam is focused normally to the interface, either grazing the edge of the nanosphere, or along the symmetry axis of the system (see Figure 14B, top). When the incidence is grazing, plasmon modes with strong rotational dependency around the symmetry axis are excited, which correspond to the Mie dipolar and higher-order modes of the single nanosphere, where the field maxima are in a plane parallel to the interface. These modes present the usual red-shift with the nanosphere radius, as shown on Figure 14B, bottom. Moreover, comparison with the carbon substrate shows that the single particle “Mie” modes are weakly affected by the nearby silver film. However, when the electron beam goes through the center of the nanosphere, a gap mode at lower energy is excited, with rotational invariance field distribution around the symmetry axis. In this gap mode, the field intensity is much enhanced inside the gap in between the particle and the film, and the scattered field has an angular distribution characteristic of a dipole perpendicular to the substrate. Note that both the silver particle and film are slightly oxidized, which gives a metal-metal distance estimated to about 4 nm in between the particle and film.

If in that previous work, only one gap mode has been found both experimentally and numerically, at least in the range of wavelength investigated, several can be supported by a nanosphere-film system. In their paper, Lei et al. [37] have investigated the plasmon properties of spherical gold particles nearly touching or partly embedded inside a gold film. Using numerical simulation (FEM) and dark field spectroscopy, they were able to characterize the different optical modes as a function of the incidence angle and the polarization of incident light (TE/TM) (see Figure 15A). They found that at least three localized modes are confined inside the gap in between the particle and the film, corresponding to different azimuthal light distribution on the nanosphere surface (see Figure 15B). The longest wavelength mode has no lateral lobes on the nanosphere edges, contrary to the two lower wavelength modes, which shows that it corresponds to the preceding gap mode with dipole perpendicular to the interface. The two lowest wavelength modes have lateral lobes, but different distribution of field around the bottom of the nanosphere. Indeed the mode labeled (1) on Figure 15B, right, shows one cancellation of the perpendicular component of the electric field whereas the mode (2) has none (see

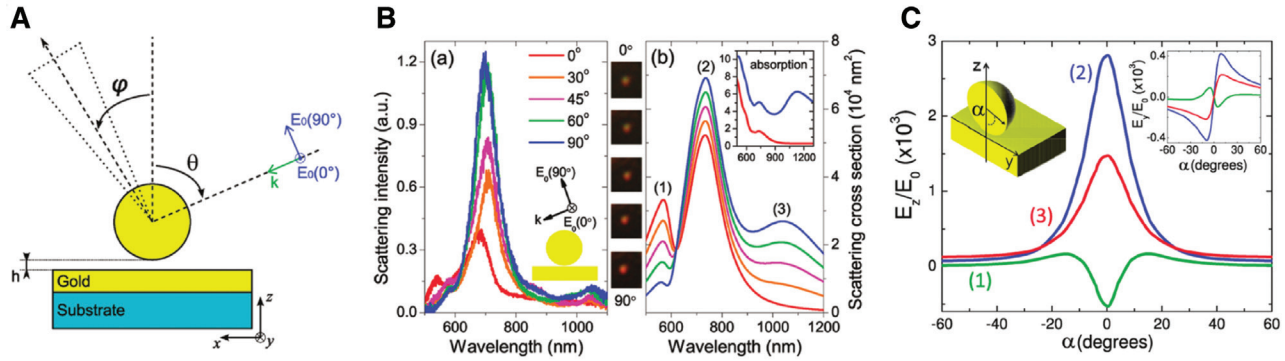

Figure 15: (A) System under investigation in [37], where a gold nanosphere is separated by a gap of size *h* from a gold film. Both the excitation and the collection are angle-dependent; (B) comparison between the experimental and simulated scattering spectra as a function of the polarization angle, together with the far-field image (dark-field spectroscopy) of the light scattered by one nanosphere; (C) distribution of the z- and y-component of the electric field around the nanosphere surface for the three modes labeled in (B). Reprinted with permission from ACS Nano, 2012, 6 (2), pp 1380–1386. Copyright 2012 American Chemical Society.

Figure 15C). Mode (2) is brighter than mode (1), and corresponds to a dipole parallel to the interface. For the partly embedded particle, two modes appear, corresponding to the excitation of two strong dipoles, one parallel to the interface and localized in the sharp angle at the junction between the particle and the film, the other perpendicular to the film.

3.2 Gap size dependency

Mock et al., investigated in 2008 the dependency of the surface plasmon modes nature and wavelength as a function of the gap thickness between a gold nanosphere and a gold film, using polyelectrolyte (PE) spacer deposited on the gold film [38] (see Figure 16A, top). The thickness of

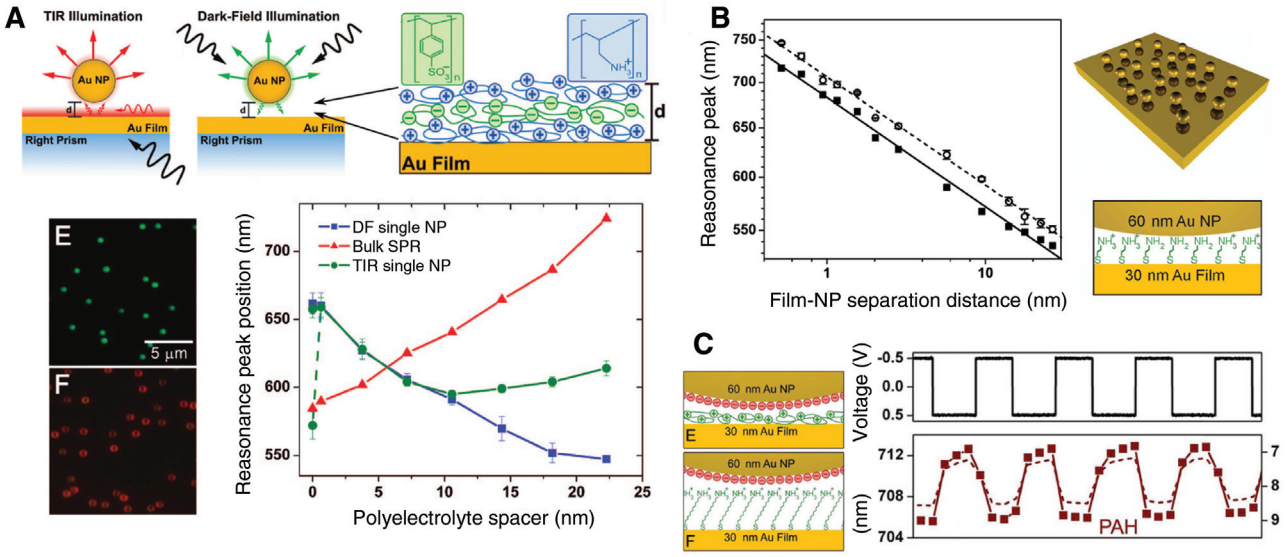

Figure 16: (A) System investigated in [38], where a gold nanosphere, separated from a gold film by a small layer of polyelectrolyte (PE), is studied either in total internal reflection (TIR) or by dark-field (DF) spectroscopy. The far-field image of the nanospheres excited in DF are shown on E and F, bottom-left, whereas the bottom-right plot shows the evolution of the different plasmon modes wavelengths with the spacer thickness, both in TIR and DF configurations; (B) evolution of the plasmon wavelength (open circles: scattering, closed squares: extinction) of an assembly of 60 nm-diameter gold nanospheres separated from a 30 nm-thick gold film by a SAM layer of thickness ranging from 1 Å to 20 Å and PE layers up to 27 nm thick, from [39]; (C) shift of the plasmon wavelength of a system similar to (2), where the thickness of the spacer is triggered by an external electric field, inducing a detectable LSP shift up to ±3 nm, from [40]. Reprinted with permission from Nano Lett., 2008, 8 (8), pp 2245–2252, ACS Nano, 2012, 6 (10), pp 9237–9246 and Nano Lett., 2012, 12 (4), pp 1757–1764. Copyright 2008 and 2012 American Chemical Society.

the PE spacer was varied from 0 nm (no PE) to about 22 nm, one PE bilayers being about 4 nm thick, and both total internal reflection (TIR) with *p* polarization and unpolarized dark field (DF) illumination were used to excite the system. The total internal reflection configuration is similar to the one investigated numerically by Lévêque and Martin in 2006 [41], the only difference being the shape of the particular which was a parallelepiped in the former. In TIR, both localized and propagative surface plasmon can be excited, whereas in DF, only the LSP modes can be directly excited, even if the light scattered by the nanoparticle can excite the PSP. When the nanosphere is placed only few nanometers above the metal film, the plasmon mode excited in DF illumination shows in the far-field a characteristic doughnut shape, which is the result of the radiation of the gap-mode with vertical dipole (see Figure 16A, bottom left, F). When the gap thickness increases, the far-field patterns looks like an Airy figure corresponding to random orientation of the emitting dipole excited inside the nanosphere (see Figure 16A, bottom left, E). When the gap decreases, DF spectroscopy shows that the LSP mode shifts to the red, even more rapidly that gap the gap is small. However, in TIR illumination, the LSP shifts to the blue, because the plasmon response is mostly modulated by the intensity of the PSP, excited by the incident *p*-polarized planewave (see Figure 16A, bottom right).

This wavelength dependency is so sensitive for a small gap that is allows to measure variations of spacer thickness with precision down to few Angstroms. In 2012, Hill et al. [39] controlled the distance between 60 nm-diameter gold nanoparticles and a 30 nm-thick gold film using self-assembled monolayers of amine-terminated alkane thiols to design the spacer, which thickness can be varied by changing the alkane chain length by step of about 1 Å from 5 Å to 20 Å (Figure 16B). The authors found a power law for the dependency of the extinction maximum wavelength with the spacer thickness as $\lambda=682.873\ d^{-0.07719}$, which gives a thickness sensitivity of 5 nm for 1 Å in the limit of very small spacers. The same year, Mock et al., demonstrated that a system of 60 nm-diameter gold spherical nanoparticles separated from a 30 nm-thick gold film by a PAH single molecular layer of about 6 Å thickness [40] could be triggered by an external electric field, inducing a detectable LSP shift up to ±3 nm (Figure 16C). The shift comes from the negatively charged citrate stabilized gold NPs which are repelled from the metal substrate when the electric field is such that the flat metal interface is negatively charged. When the electric field is reversed, the metal interface is charged positively and the NS is attracted to the metal film, reducing the gap and shifting the plasmon wavelength slightly to the red.

3.3 Quantum regime

When the distance between the particle and the metal film becomes on the scale of 1 nm and less, classical theory predicts an extreme field enhancement of several orders of magnitude compared to the incident field, together with a large redshift of the plasmon wavelength. Corrections must be brought to the so-called “local” description of the optical response of the metal, where the dielectric constant is supposed to depend only on the angular frequency of the electromagnetic field but not on its wavevector. These corrections result from the quantum repulsion between the electron gas near the interface between two nearly touching metal systems (Pauli exclusion principle) together with the possibility of quantum tunneling across the gap (which efficiency at optical frequencies is questionable [42]).

As stated by Ciracì et al. [43], a full treatment of the optical response for small gap is only possible for very small spheres, that is why it is crucial to develop semi-empirical models that can be applied to larger systems. They demonstrated that the hydrodynamic description of the collective motion of the electrons in the metal allows, by taking into account the quantum pressure due to the repulsion, to successfully reproduce the experimental shift of the plasmon peak of particle-film system separated by a gap of 0.1 nm–30 nm, obtained using SAMs and layer-by-layer deposition (Figure 17A). Indeed, while the local theory predicts a wavelength of 900 nm as a limit of zero gap, the experiment gives 750 nm. The model of quantum repulsion pressure consists in the description of the electron gas near the metal surface as not infinitely thin but spread over a finite thickness across the boundary. The extent of the charge density is given by the Thomas-Fermi screening length $\lambda_{TF}=\beta/\omega_p$, where β is a factor proportional to the Fermi velocity and ω_p is the bulk plasmon frequency of the metal, which is on the order of 1 Å. Figure 17B shows the comparison between the local theory and the hydrodynamic model with different values of β on the evolution of both the resonance wavelength and the enhancement factor with the gap: the local theory clearly overestimates both for gap larger than 1 nm.

4 Applications

4.1 Towards perfect black absorbers…

Until now, the greater potential of Au coupled NPs-films systems probably lies in the fabrication and design of

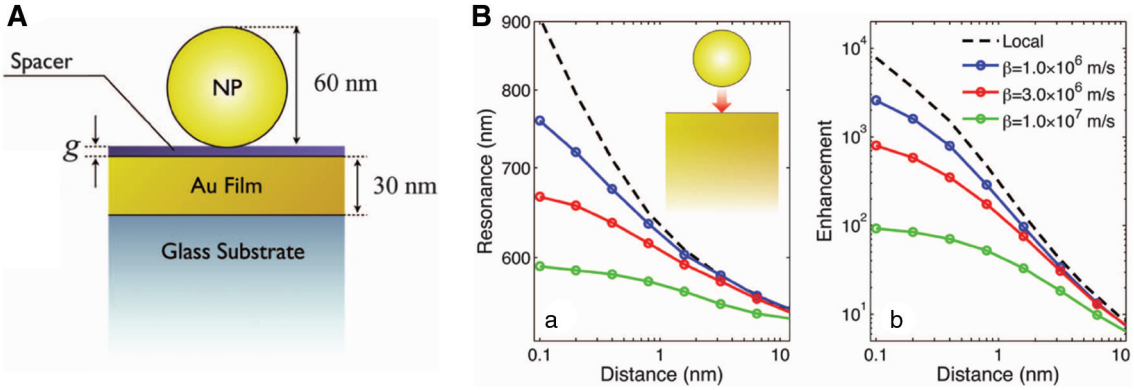

Figure 17: (A) System theoretically investigated in [43], where the nanosphere is separated from the metal film by a gap with size down to 1 Å; (B) both the plasmon mode wavelength and the field enhancement in the gap have been calculated with an hydrodynamic model, where β is a parameter proportional to the Fermi velocity. From C. Ciracì, R. T. Hill, J. J. Mock, Y. Urzhumov, A. I. Fernández-Domínguez, S. A. Maier, J. B. Pendry, A. Chilkoti and D. R. Smith, Probing the ultimate limits of plasmonic enhancement., Science, vol. 337,n°6098, pp. 1072–4 (2012). Reprinted with permission from AAAS.

perfect black absorbers. Indeed, for the past few years, this topic has deserved much more attention from several leading groups. The objective is to take advantage of NP-film coupling in order to design advanced metamaterials absorbing light at optical frequencies over a broad wavelength range. Such perfect absorbers could be of great interest for harvesting solar energy.

In 2010, Hao et al., performed FDTD simulations to design efficient optical absorbers consisted in a layer of gold particles and a gold film separated by a Al_2O_3 dielectric spacer [44]. They showed that such systems play the role of ultra-thin, wide-angle, subwavelength, high performance metamaterial absorber for optical frequencies. Experimentally, they showed an 88% absorption peak at the wavelength of 1.58 μm for TM polarized light (see Figure 18). From the FDTD simulations, it has been shown that the optimal spacer thickness is around 10 nm. From the authors, such strong absorption comes from the excitation of localized magnetic and electric dipoles which conducts to light trapping and its dissipation by ohmic losses.

Continuing this pioneering work and others [45], Moreau et al., have focused on gap modes between Ag nanocubes and an Au film to fabricate controlled-reflectance surfaces [46]. As is well illustrated in this communication, perfect absorber are systems with no reflectance

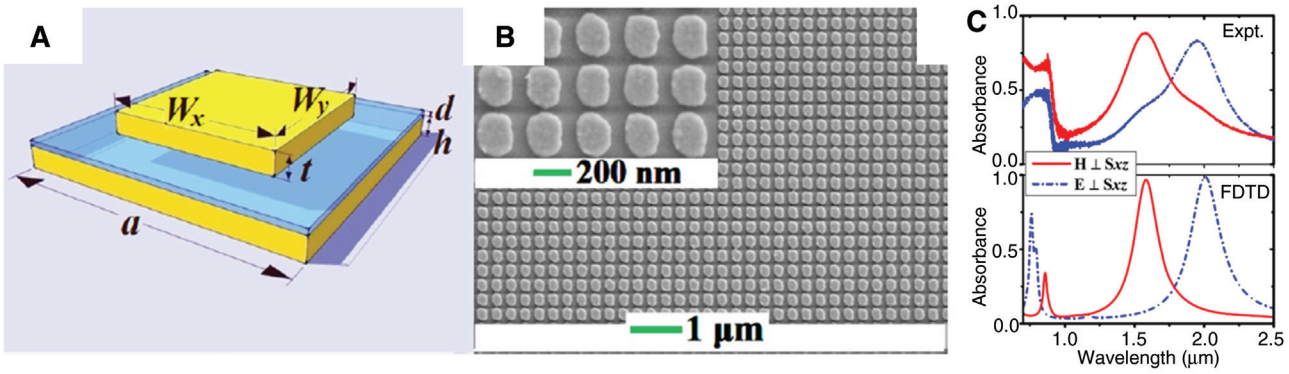

Figure 18: (A) Geometry of the sample studied by Hao et al. [44], W_x and W_y represent, respectively, the side lengths of rectangular Au particles along the x and y axis and t represents its thickness. d and h, respectively, denote the thicknesses of the Al_2O_3 dielectric spacer and the gold film. a is the lattice constant. (B) Top view SEM image of the fabricated optical metamaterial absorber. (C) Measured and simulated absorbance spectra for a sample with W_x=170 nm, W_y=230 nm, t=40 nm, d=10 nm, h=50 nm, and a=310 nm at 20° angle of incidence. For TM polarized light, the maximum absorption of 88% is obtained at the wavelength 1.58 μm while for the case of TE polarized light, the maximum absorption can be as high as 83% and the resonance wavelength is shifted to 1.95 μm. Reprinted with permission from Appl. Phys. Lett., vol. 96, pp. 251104–251104–3, 2010. Copyright 2010 American Institute of Physics.

and no transmittance. If metal substrates may easily not transmit incident light, suppressing reflectance is much harder and requires the fabrication of metasurfaces. To achieve such an objective, it is necessary to match the wave impedance $z_j = \sqrt{\mu_j / \varepsilon_j}$ of the medium. As artificially structured metamaterials can provide tunable magnetic as well as electric properties [47], they appear to be ideal candidates of designing perfect light absorbers. As explained by Moreau et al., the trick consists of designing materials which will support both electric and fictious magnetic current densities when they are excited by incident light but both lying at the root of reflected waves which are exactly out of phase. Simulations performed by Moreau et al., in order to study gap modes between Ag nanocubes and an Au film separated by a dielectric spacer with a refractive index of 1.54, showed that the most suitable spacer thickness for designing optical absorbers is comprised between 5 nm and 10 nm in agreement with [44]. Moreover, they demonstrated that no complex nanofabrication process is required as the chemically synthesized Ag nanocubes can just be randomly deposited onto the gold film coated with the dielectric layer, therefore providing large tunable reflectance surfaces. Moreover it must be noted that low surface coverage, around 17%, is required to achieve reflectance lower than 7% (see Figure 19).

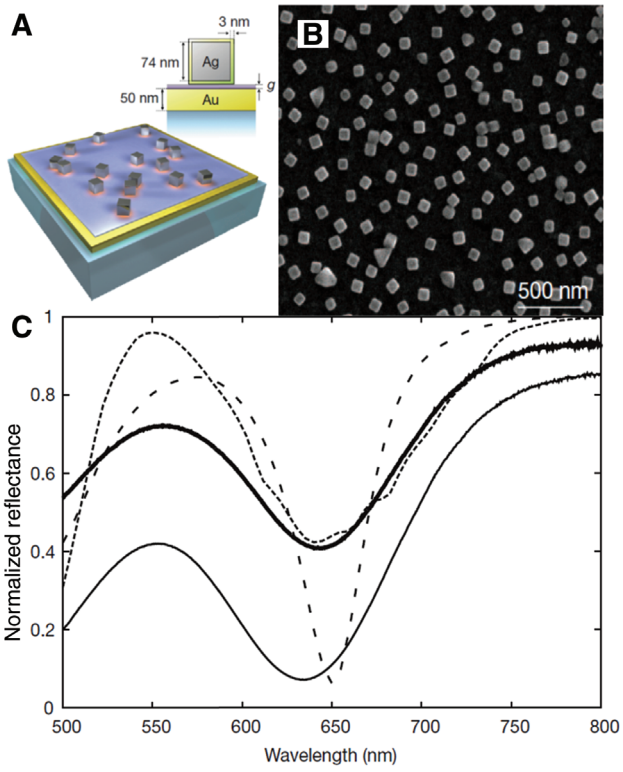

Figure 19: (A) Geometry of the sample studied by Moreau et al. [46]. Tunable reflectance surfaces may be fabricated by covering gold film with Ag nanocubes separated by a 10 nm polymer spacer layer (n=1.54). (B) Top view SEM image of the fabricated optical metamaterial absorber. (C) Experimental reflectance for normal incidence, normalized to the gold film, for surface coverages of 7.3% (thin solid line) and 17.1% (thick solid line), compared with simulations of uniform cubes (4.2% surface coverage, dotted line) and a model including size dispersion (dashed line, see details included in [46]). Reprinted by permission from Macmillan Publishers Ltd: [NATURE] (A. Moreau, C. Ciracì, J. J. Mock, R. T. Hill, Q. Wang, B. J. Wiley, A. Chilkoti, D. R. Smith, and C. Ciraci, Controlled-reflectance surfaces with film-coupled colloidal nanoantennas, Nature, vol. 492, n°. 7427, pp. 86–89 (2012)), copyright (2012).

At the same time, Nielsen et al. took advantage of gap plasmon resonators (GPR) to fabricate optical absorbers over a broad range of optical wavelengths (see Figure 20). Indeed, by fabricating a continuous layer of GPR (CL-GPR) with different sizes, they obtained an average 94% of absorption in the entire visible wavelength range (400–750 nm) [48]. The great interest of GPR consisted in plasmonic nanostructures separated from a plasmonic film by a dielectric layer is that the associated GPRs are almost independent from the incident angle. The chosen dielectric spacer thickness for this metamaterial made of plasmonic NPs coupled to plasmonic film is 20 nm.

Recently, M. Elbahri and coworkers succeeded in designing and fabricating a perfect absorber showing almost 100% absorbance over a broad range of wavelengths from UV to near-IR and which can be even coated on a flexible polymer [49]. The perfect absorber can be either coated on a glass or flexible substrate (see Figure 21). The fabrication process proposed by Elbahri and coworkers is cost-effective and offers high absorption on the whole visible spectrum. Another lithography-free process was also proposed by Yan et al. [50] and provides an alternative for mass and cost-effective production. The process for making large areas of nanoparticles on top of the gold film coated with the dielectric layer consists in thermal annealing of a thin gold film. Such processes make black reflectors appealing for applications as absorber or anti-reflection coatings [51]. Moreover, the ability of such systems for light trapping makes them ideal candidates for silicon solar cells as demonstrated by H. Tan and coworkers [52].

4.2 … and perfect transmittance

As shown in the previous section, Elbahri and coworkers designed perfect absorbers by incorporating a 25 nm dielectric spacer between a gold film and an Au/SiO_2 nanocomposite film [49]. In the same time, they studied similar systems but without the dielectric spacer [53] and fabricated

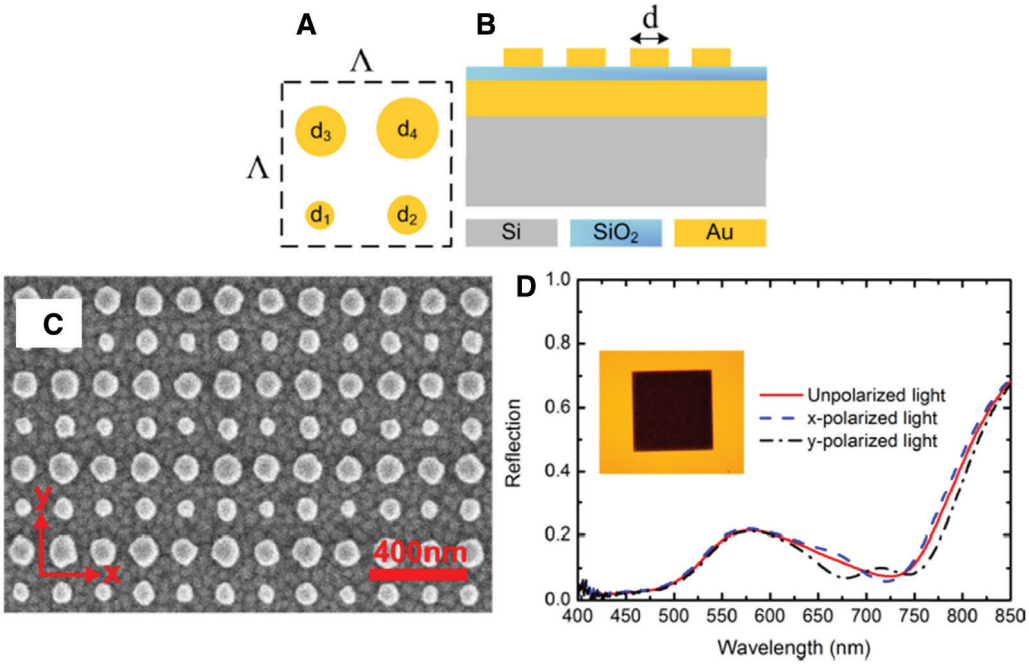

Figure 20: (A) Geometry of the sample studied by Nielsen et al. [48]. The unit cell is quadratic of size Λ and contains four gold nanoparticles with different diameters. (B) Schematic representation of the layered sample structure. (C) Top-view SEM image of the fabricated CL-GPRs with particle diameters d1=60 nm, d2=80 nm, d3=100 nm and d4=120 nm and unit-cell size Λ=340 nm. (d) Reflection spectra for unpolarized (solid red curve), x-polarized (dashed blue curve) and y-polarized (black dash-dotted curve) light. The inset shows a microscope image of the 30 μm×30 μm CL-GPR array for unpolarized light and its appearance compared to the surrounding smooth gold film coated with ~20 nm SiO_2. Reprinted figure with permission from M. G. Nielsen, A. Pors, O. Albrektsen, and S. I. Bozhevolnyi, Optics Express, vol. 20, pp. 13311 (2012). Copyright 2012 by the Optical Society (OSA).

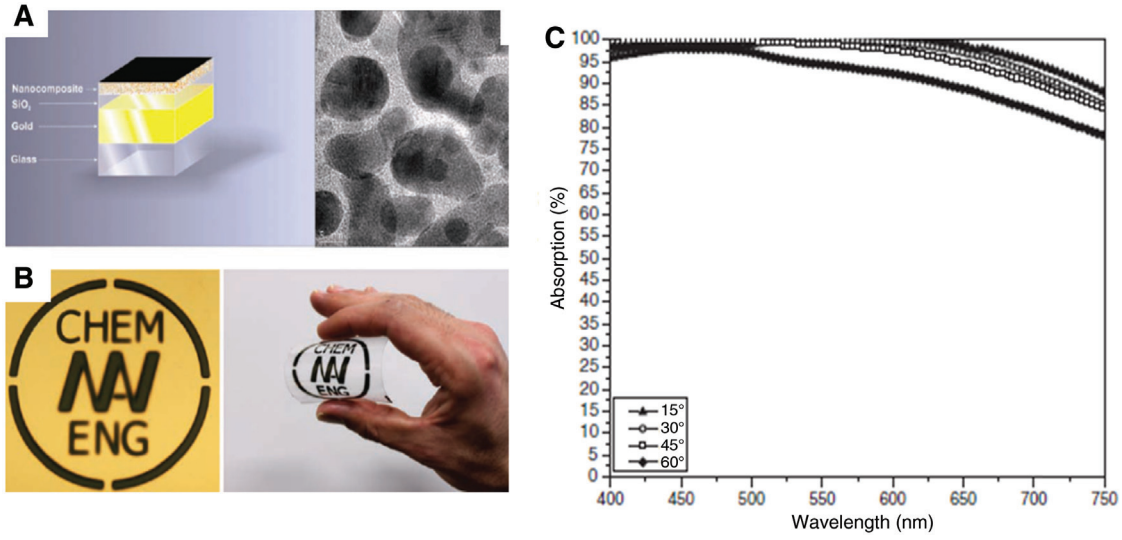

Figure 21: (A) Geometry of the sample studied by Elbahri and coworkers [49]. The structure is composed of (from bottom to the top) a glass substrate coated with an optically thick (100 nm) Au film followed by a thin (25 nm) dielectric layer (SiO_2) acting as the spacer layer and at the very top, a thin (20 nm) nearly percolated film of nanocomposite (Au/SiO_2).The left panel illustrates that the whole structure resides on a glass substrate; the right panel shows a top-view TEM image of the nanocomposite film. (B) The perfect absorber (blackbody) can be coated via a mask either on gold-coated glass (left) or on flexible polymer foil (right). (C) Absorption spectra of the perfect absorber shown in (A) and (B) with TM polarization at different angles of incidence. Reprinted with permission from Adv. Mater., vol. 23, pp. 5410–4, 2011. Copyright 2011 John Wiley and Sons.

the first transparent conducting metal (TCM). The system is composed of glass coated with a thin (25 nm) gold film and a polymer containing silver nanoparticles. This plasmonic metamaterial exhibits optical transmission up to 80% in the visible wavelength range (see Figure 22), comparable with ITO's transparency, and electric conductivity

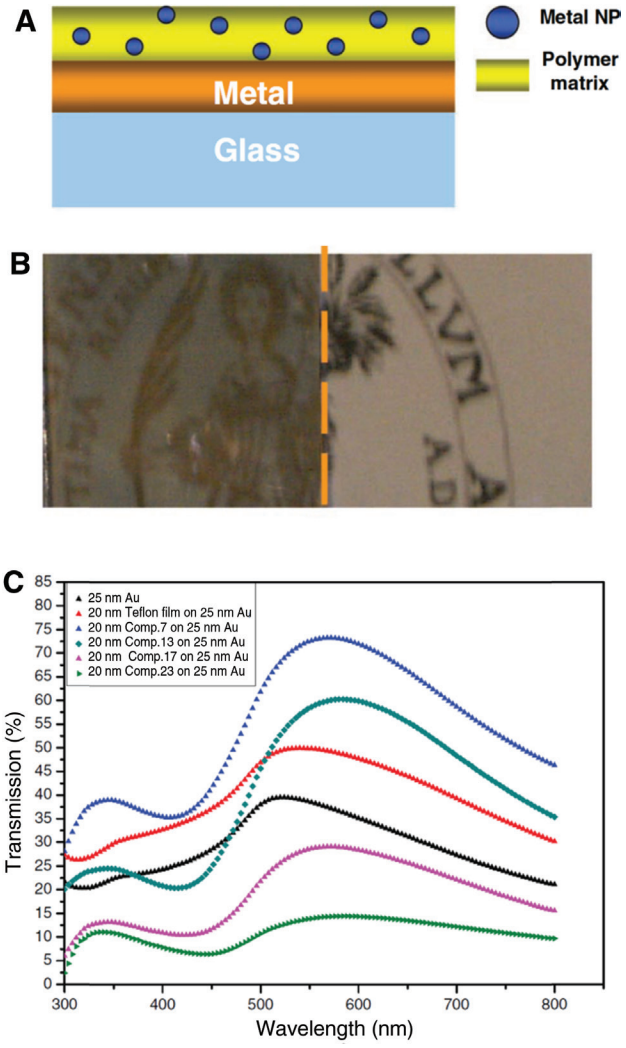

Figure 22: (A) Geometry of the sample studied by Elbahri and coworkers [53]. The structure is composed of glass coated with a thin (25 nm) gold film and a polymer containing silver nanoparticles. (B) Photograph of the Christian-Albrechts University logo taken through a glass piece coated with a 25 nm gold film (left) and 20 nm Comp.7 on a 25-nm gold fi lm (right). Comp. 7 means the nanocomposite sample with 7 wt% of gold nanoparticles. (C) Transmission spectra for the sample arrangement shown in (A) with 7 vol%, 13 vol%, 17 vol%, and 23 vol% filling factors of the nanocomposite layer. The uncoated 25 nm gold film and the 20 nm Teflon film coated on a 25 nm gold film are shown as references. Reprinted with permission from Adv. Mater., vol. 23, pp. 1993–1997, 2011. Copyright 2011 John Wiley and Sons.

one order higher than ITO's one. Meanwhile, Liu et al., led a full numerical study on continuous film with double plasmonic arrays that is to say one non-close-packed Au sphere array both on its top and its bottom. They showed that such coupled NP-film could conduct to near-unit transparency devices [54]. Recently, they also showed the possibility to take advantage of the coupling between Ag film and Ag/SiO_2/Ag nanoparticles to design multispectral optical enhanced transmission devices [55].

4.3 Towards plasmonic waveguides for biosensing

Another technological potential for plasmonic NP-film coupled systems remains the design and fabrication of plasmonic waveguides. Continuing their work concerning perfect absorbers, Smith and coworkers showed that film-coupled nanocube systems exibit interesting optical properties for tunable reflectance or chemical sensing due to the formation of waveguide cavity-like modes between the silver nanocubes and the gold film [35]. At the same time, Cui et al., proposed to take advantage of coupling between localized surface plasmon of metallic particle chains and PSP modes of plasmonic films in order to guide light and enhance performances of biosensors and surface enhanced spectroscopy applications [56]. Ten years previously, Daniels and Chumanov already showed that the plasmon coupling between a silver mirror film and silver nanoparticles, as well as Murphy and co-workers with gold nanoparticles self-assembled onto gold film [57], could lead to a significant Raman enhancement making such system ideal applicant for SERS biosensors [58]. Usually, Au NPs aggregates or dimmers are known to be excellent SERS substrates. Recently, Moskovits and coworkers evidenced the NP-overmirror (NPOM) – that is to say NPs on top of au film coated with a thin dielectric layer – allows SERS signal enhancement by a factor 10 even for aggregates [59]. Wang et al., confirmed these results by focusing – both numerically and experimentally – on SERS gap modes when molecules are located in-between au NP dimmers and Au film [60]. As for LSP biosensors, T. Maurer and coworkers evidenced a FoM (figure of merit) as high as 2.8 for Au NP gratings – Au film systems coupled via a trilayer graphene spacer [61, 62] exhibiting LSP at about 520 nm which ranks such LSP sensors among the more sensitive for those whose localized surface plasmon resonance is in the visible range [63]. Indeed, most of the interfaces with high FoM (4–16.5) [16, 63, 64] take advantage of the fact that higher sensitivities are achieved with plasmon bands in the near-infrared of the spectrum (850–1200 nm).

Among the most sensitive sensors in the near-IR range, Au rings-Au film coupled systems provide foM as high as 16 for phase measurements [64].

5 Conclusion and outlook

The renewed interest in coupled plasmonic film-nanoparticles systems is fully justified by the richness and variety of modes which can be exhibited and which leads to the tunability of optical absorption when modes hybridize. Indeed, propagative PSP of the plasmonic film can be excited by nanoparticle gratings. The resonance wavelength of propagative PSP is closely related to the grating pitches and can therefore hybridize with LSP of nanoparticles when both resonance wavelengths match. Moreover, another interesting feature of such complex systems remains in the excitation of a low wavelength localized mode, at 525 nm, whose wavelength is fairly independent of nanoparticle diameter or inter-particle distances, though the exact physical origin of the mode remains unclear (vertical LSP mode, quadrupolar mode ...). Such plasmonic modes have been evidenced to be relevant for biosensing. Moreover, both for plasmonic films coupled to single/random nanoparticles or regulars arrays of nanoparticles, when the spacer layer is decreased, gap modes appear leading to strong absorption of light. By playing with the size of nanoparticles deposited onto the plasmonic film coated with a dielectric spacer layer, it becomes possible to design perfect absorbers over a large wavelength range, known as black gold. This is probably one of the most promising applications of such coupled systems. In the next future, we believe that what is at stake remains the tunability of hybridization between the different plasmonic modes by playing on both 2D-arrangement of nanoparticles and the spacer layer thickness and index of refraction.

Acknowledgments: T. M. thanks the DRRT (Délégation Régionale à la Recherche et à la Technologie) of Champagne-Ardenne, the Labex ACTION project (contract ANR-11-LABX-01-01) and the CNRS via the chair of "optical nanosensors" for financial support. This work was performed in the context of the COST Action MP1302 Nanospectroscopy.

References

[1] Barnes WL, Dereux A, Ebbesen TW. Surface plasmon subwavelength optics. Nature 2003;424:824–30.

[2] Bergman DJ, Stockman MI. Surface plasmon amplification by stimulated emission of radiation: quantum generation of coherent surface plasmons in nanosystems. Phys Rev Lett 2003;90:027402.

[3] Szunerits S, Boukherroub R. Sensing using localised surface plasmon resonance sensors. Chem Commun (Camb). 2012;48:8999–9010.

[4] Huang X, Jain PK, El-Sayed IH, El-Sayed MA. Plasmonic photothermal therapy (PPTT) using gold nanoparticles. Laser Med Sci 2008;23:217–28.

[5] Hayashi S, Okamoto T. Plasmonics: visit the past to know the future. J Phys D: Appl Phys 2012;45:433001.

[6] Liu Y, Zhang X. Metamaterials: a new frontier of science and technology. Chem Soc Rev. 2011;40:2494–507.

[7] Bohren CF, Huffman DR. Absorption and scattering of light by small particles. (Wiley science paperback series), vol. 16. 1998:544.

[8] Martin OJF. "Plasmon Resonances in Nanowires with a Non-regular Cross-Section," in *Optical Nanotechnologies The Manipulation of Surface and Local Plasmons*, vol. 210, 2003, pp. 183–210.

[9] Novotny L, van Hulst N. Antennas for light. Nat Photon 2011;5:83–90.

[10] Bohren CF, Huffman DR. Absorption and scattering of light by small particles. Weinheim, Germany: Wiley-VCH Verlag GmbH, 1998.

[11] Fuchs R. Theory of the optical properties of ionic crystal cubes. Phys Rev B 1975;11:1732–40.

[12] Zhang S, Bao K, Halas NJ, Xu H, Nordlander P. Substrate-induced Fano resonances of a plasmonic nanocube: a route to increased-sensitivity localized surface plasmon resonance sensors revealed. Nano Lett 2011;11:1657–3.

[13] Schmidt F-P, Ditlbacher H, Hohenester U, Hohenau A, Hofer F, Krenn JR. Dark plasmonic breathing modes in silver nanodisks. Nano Lett 2012;12:5780–3.

[14] Luk'yanchuk B, Zheludev NI, Maier SA, Halas NJ, Nordlander P, Giessen H, Chong CT. The Fano resonance in plasmonic nanostructures and metamaterials. Nat Mater 2010;9:707–15.

[15] Lovera A, Gallinet B, Nordlander P, Martin OJF. Mechanisms of Fano resonances in coupled plasmonic systems. ACS Nano 2013;7:4527–36.

[16] Verellen N, Van Dorpe P, Huang C, Lodewijks K, Vandenbosch GAE, Lagae L, Moshchalkov VV. Plasmon line shaping using nanocrosses for high sensitivity localized surface plasmon resonance sensing. Nano Lett 2011;11:391–7.

[17] Nylander C, Liedberg B, Lind T. Gas detection by means of surface plasmon resonance. Sensor Actuator 1982;3:79–88.

[18] Baudrion A-L, de Léon-Pérez F, Mahboub O, Hohenau A, Ditlbacher H, García-Vidal FJ, Dintinger J, Ebbesen TW, Martin-Moreno L, Krenn JR. Coupling efficiency of light to surface plasmon polariton for single subwavelength holes in a gold film. Opt Express 2008;16:3420–9.

[19] Lopez-Tejeira F, Rodrigo SG, Martin-Moreno L, Garcia-Vidal FJ, Devaux E, Dintinger J, Ebbesen TW, Krenn JR, Radko IP, Bozhevolnyi SI, Gonzalez MU, Weeber JC, Dereux A. Modulation of surface plasmon coupling-in by one-dimensional surface corrugation. 2007;033035:20.

[20] Ropers C, Neacsu CC, Elsaesser T, Albrechty M, Raschke MB, Lienau C. Grating-coupling of surface plasmons onto metallic tips: a nanoconfined light source. Nano Lett 2007;7:2784–8.

[21] Lamy J-M, Justice J, Lévêque G, Corbett B. Monolithic excitation and manipulation of surface plasmon polaritons on a vertical cavity surface emitting laser Appl Phys A 2011;103:665–7.
[22] Lalanne P, Hugonin JP. Interaction between optical nano-objects at metallo-dielectric interfaces. 2006;Nat Phys 2:551–6.
[23] Berini P. Long-range surface plasmon polaritons. Adv Opt Photonics 2009;1:484.
[24] Krupin O, Asiri H, Wang C, Tait RN, Berini P. Biosensing using straight long-range surface plasmon waveguides. Opt Express 2013;21:698–709.
[25] Farhang A, Martin OJF. Plasmon delocalization onset in finite sized nanostructures. Opt Express 2011;19:11387–96.
[26] Holland WR, Hall DG. Surface-plasmon dispersion relation: Shifts induced by the interaction with localized plasma resonances. Phys Rev B 1983;27:7765–8.
[27] Kume T, Hayashi S, Yamamoto K. Light emission from surface plasmon polaritons mediated by metallic fine particles. Phys Rev B 1997;55:4774–82.
[28] Holland WR, Hall DG. Frequency shifts of an electric-dipole resonance near a conducting surface. Phys Rev Lett 1984;52:1041–4.
[29] Stuart H, Hall D. Enhanced dipole-dipole interaction between elementary radiators near a surface. Phys Rev Lett 1998;80:5663–6.
[30] Félidj N, Aubard J, Lévi G, Krenn JR, Schider G, Leitner A, Aussenegg FR. Enhanced substrate-induced coupling in two-dimensional gold nanoparticle arrays. Phys Rev B 2002;66:245407.
[31] Hohenau A, Krenn JR. Plasmonic modes of gold nano-particle arrays on thin gold films. Phys Status Solidi – Rapid Res Lett 2010;4:256–8.
[32] Linden S, Kuhl J, Giessen H. Controlling the interaction between light and gold nanoparticles: selective suppression of extinction. Phys Rev Lett 2001;86:4688–91.
[33] Cesario J, Quidant R, Badenes G, Enoch S. Electromagnetic coupling between a metal nanoparticle grating and a metallic surface. Opt Lett 2005;30:3404–6.
[34] Farhang A, Siegfried T, Ekinci Y, Sigg H, Martin OJF. Large-scale sub-100 nm compound plasmonic grating arrays to control the interaction between localized and propagating plasmons. J Nanophotonics 2014;8:083897.
[35] Lassiter JB, McGuire F, Mock JJ, Ciracì C, Hill RT, Wiley BJ, Chilkoti A, Smith DR. Plasmonic waveguide modes of film-coupled metallic nanocubes. Nano Lett 2013;13:5866–72.
[36] Yamamoto N, Ohtani S, Garcia De Abajo FJ. Gap and mie plasmons in individual silver nanospheres near a silver surface. Nano Lett 2011;11:91–5.
[37] Lei DY, Fernández-Domínguez AI, Sonnefraud Y, Appavoo K, Haglund RF, Pendry JB, Maier SA. Revealing plasmonic gap modes in particle-on-film systems using dark-field spectroscopy. ACS Nano 2012;6:1380–6.
[38] Mock JJ, Hill RT, Degiron A, Zauscher S, Chilkoti A, Smith DR. Distance-dependent plasmon resonant coupling between a gold nanoparticle and gold film. Nano Lett 2008;8:2245–52.
[39] Hill RT, Mock JJ, Hucknall A, Wolter SD, Jokerst NM, Smith DR, Chilkoti A. Plasmon ruler with angstrom length resolution. ACS Nano 2012;6:9237–46.
[40] Mock JJ, Hill RT, Tsai Y-J, Chilkoti A, Smith DR. Probing dynamically tunable localized surface plasmon resonances of film-coupled nanoparticles by evanescent wave excitation. Nano Lett 2012;12:1757–64.
[41] Lévêque G, Martin OJF. Optical interactions in a plasmonic particle coupled to a metallic film. Opt Express 2006;14:9971–81.
[42] Mortensen NA, Raza S, Wubs M, Søndergaard T, Bozhevolnyi SI. A generalized non-local optical response theory for plasmonic nanostructures. Nat Commun 2014;5:3809.
[43] Ciracì C, Hill RT, Mock JJ, Urzhumov Y, Fernández-Domínguez AI, Maier SA, Pendry JB, Chilkoti A, Smith DR. Probing the ultimate limits of plasmonic enhancement. Science 2012;337:1072–4.
[44] Hao J, Wang J, Liu X, Padilla WJ, Zhou L, Qiu M. High performance optical absorber based on a plasmonic metamaterial. Appl Phys Lett 2010;96:251104–251104–3.
[45] Wu C, Neuner B, Shvets G, John J, Milder A, Zollars B, Savoy S. Large-area wide-angle spectrally selective plasmonic absorber. Phys Rev B 2011; 84:075102.
[46] Moreau A, Ciracì C, Mock JJ, Hill RT, Wang Q, Wiley BJ, Chilkoti A, Smith DR, Ciraci C. Controlled-reflectance surfaces with film-coupled colloidal nanoantennas. Nature 2012;492:86–9.
[47] Shalaev VM. Optical negative-index metamaterials. Nat Photonics 2007;1:41–8.
[48] Nielsen MG, Pors A, Albrektsen O, Bozhevolnyi SI. Efficient absorption of visible radiation by gap plasmon resonators. Opt Express 2012;20:13311.
[49] Hedayati MK, Javaherirahim M, Mozooni B, Abdelaziz R, Tavassolizadeh A, Chakravadhanula VSK, Zaporojtchenko V, Strunkus T, Faupel F, Elbahri M. Design of a perfect black absorber at visible frequencies using plasmonic metamaterials. Adv Mater 2011;23:5410–4.
[50] Yan M, Dai J, Qiu M. Lithography-free broadband visible light absorber based on a mono-layer of gold nanoparticles. J Opt 2014;16:25002.
[51] Liu G-Q, Liu Z-Q, Huang K, Chen Y-H, Cai Z-J, Zhang X-N, Hu Y. Narrowband light total antireflection and absorption in metal film–array structures by plasmonic near-field coupling. Plasmonics 2014;9:17–25.
[52] Tan H, Santbergen R, Smets AHM, Zeman M. Plasmonic light trapping in thin-film silicon solar cells with improved self-assembled silver nanoparticles. Nano Lett. 2012;12:4070–6.
[53] Elbahri M, Hedayati MK, Kiran Chakravadhanula VS, Jamali M, Strunkus T, Zaporojtchenko V, Faupel F. An omnidirectional transparent conducting-metal-based plasmonic nanocomposite. Adv Mater 2011;23:1993–7.
[54] Liu Z, Liu G, Zhou H, Liu X, Huang K, Chen Y, Fu G. Near-unity transparency of a continuous metal film via cooperative effects of double plasmonic arrays. Nanotechnology 2013;24:155203.
[55] Liu GQ, Hu Y, Liu ZQ, Cai ZJ, Zhang XN, Chen YH, Huang K. Multispectral optical enhanced transmission of a continuous metal film coated with a plasmonic core-shell nanoparticle array. Opt Commun 2014;316:111–9.
[56] Cui L, Song G, Lang P, Wu C, Liu H, Yu L, Xiao J. Optical interaction in a plasmonic metallic particle chain coupled to a metallic film. Optik (Stuttg) 2013;124:6936–8.
[57] Orendorff CJ, Gole A, Sau TK, Murphy CJ. Surface-enhanced raman spectroscopy of self-assembled monolayers: sandwich architecture and nanoparticle shape dependence. Anal Chem 2005;77:3261–6.
[58] Daniels JK, Chumanov G. Nanoparticle-mirror sandwich substrates for surface-enhanced Raman scattering. J Phys Chem B 2005;109:17936–42.

[59] Mubeen S, Zhang S, Kim N, Lee S, Krämer S, Xu H, Moskovits M. Plasmonic properties of gold nanoparticles separated from a gold mirror by an ultrathin oxide. Nano Lett 2012;12:2088–94.
[60] Wang X, Li M, Meng L, Lin K, Feng J, Huang T, Yang Z, Ren B. Probing the location of hot spots by surface-enhanced Raman spectroscopy: toward uniform substrates. ACS Nano 2014;8:528–36.
[61] Maurer T, Nicolas R, Leveque G, Subramanian P, Proust J, Béal J, Schuermans S, Vilcot JP, Herro Z, Kazan M, Plain J, Boukherroub R, Akjouj A, Djafari-Rouhani B, Adam PM, Szunerits S. Enhancing LSPR sensitivity of Au gratings through graphene coupling to Au film. Plasmonics 2013;9:507–12.
[62] Nicolas R, Maurer T, Lévêque G, Subramanian P, Proust J, Béal J, Schuermans S, Vilcot J-P, Herro Z, Kazan M, Plain J, Boukherroub R, Akjouj A, Djafari-Rouhani B, Adam P-M, Szunerits S. Enhanced gold film-coupled graphene-based plasmonic nanosensor. Proceeding SPIE, Plasmon Met Nanostructures Their Opt Prop XI 2013;8809:88090R.
[63] Zalyubovskiy SJ, Bogdanova M, Deinega A, Lozovik Y, Pris AD, An KH, Hall WP, Potyrailo RA. Theoretical limit of localized surface plasmon resonance sensitivity to local refractive index change and its comparison to conventional surface plasmon resonance sensor. J Opt Soc Am A 2012;29:994–1002.
[64] Lodewijks K, Van Roy W, Borghs G, Lagae L, Van Dorpe P. Boosting the figure-of-merit of LSPR-based refractive index sensing by phase-sensitive measurements. Nano Lett 2012;12:1655–9.